Association of Tropical Cirrus in the 10–15-km Layer with Deep Convective Sources: An Observational Study Combining Millimeter Radar Data and Satellite-Derived Trajectories

GERALD G. MACE AND MIN DENG

University of Utah, Salt Lake City, Utah

BRIAN SODEN

Geophysical Fluid Dynamics Laboratory, Princeton, New Jersey

ED ZIPSER

University of Utah, Salt Lake City, Utah

(Manuscript received 12 October 2004, in final form 20 May 2005)

ABSTRACT

In this paper, millimeter cloud radar (MMCR) and Geosynchronous Meteorological Satellite (GMS) data are combined to study the properties of tropical cirrus that are common in the 10–15-km layer of the tropical troposphere in the western Pacific. Millimeter cloud radar observations collected by the Atmospheric Radiation Measurement program on the islands of Manus and Nauru in the western and central equatorial Pacific during a 12-month period spanning 1999 and 2000 show differences in cirrus properties: over Manus, where clouds above 7 km are observed 48% of the time, the cirrus are thicker and warmer on average and the radar reflectivity and Doppler velocity are larger; over Nauru clouds above 7 km are observed 23% of time. To explain the differences in cloud properties, the relationship between tropical cirrus and deep convection is examined by combining the radar observations with GMS satellite-derived back trajectories. Using a data record of 1 yr, it is found that 47% of the cirrus observed over Manus can be traced to a deep convective source within the past 12 h while just 16% of the cirrus observed over Nauru appear to have a convective source within the previous 12 h. Of the cirrus that can be traced to deep convection, the evolution of the radar-observed cloud properties is examined as a function of apparent cloud age. The radar Doppler moments and ice water path of the observed cirrus at both sites generally decrease as the cirrus age increase. At Manus, it is found that cirrus during boreal winter typically advect over the site from the southeast from convection associated with the winter monsoon, while during boreal summer, the trajectories are mainly from the northeast. The properties of these two populations of cirrus are found to be different, with the winter cirrus having higher concentrations of smaller particles. Examining statistics of the regional convection using Tropical Rainfall Measuring Mission (TRMM), it is found that the properties of the winter monsoon convection in the cirrus source region are consistent with more intense convection compared to the convection in the summer source region.

1. Introduction

Upper-tropospheric ice-phase clouds in the Tropics (hereafter referred to as tropical cirrus) are characterized by their extensive lateral and vertical coverage. These clouds impose a substantial large-scale radiative effect on the earth's climate system (Hartmann 1993). Up to 20% of the global Tropics are regularly covered by extensive cirrus systems (Liou 1986), and these cloud layers reduce the solar radiation reaching the earth's surface due to reflection. These cloud layers also absorb a portion of the upwelling infrared (IR) radiation emitted by the surface and lower atmosphere and emit IR radiation at a much lower temperature, hence effectively reducing the outgoing longwave radiation (OLR) and heating the atmosphere. The net radiative effect of tropical cirrus depends on several

Corresponding author address: Gerald G. Mace, Dept. of Meteorology, University of Utah, 135 S 1460 E, Rm 819 (819 WBB), Salt Lake City, UT 84112-0110.
E-mail: mace@met.utah.edu

© 2006 American Meteorological Society

factors including the properties of the underlying surface and atmosphere (Stephens et al. 1990), the cloud amount, cloud height, cloud geometrical thickness, ice water content (IWC), and the details of the ice crystal size distribution (Stephens 2005). Tropical cirrus clouds, in particular, can have a unique tendency to produce positive heating anomalies in the troposphere (Ackerman et al. 1988).

Cirrus also play a role in the maintenance of the water vapor distribution in the Tropics. In the regions of general subsidence well removed from deep convection, cirrus moisten the upper troposphere and, thereby, regulate the heating rates and large-scale vertical motions of the Tropics (e.g., Sherwood 1996). In the vertical region bounded by the detrainment layer of deep convection and the stratosphere known as the tropopause transition layer (TTL), tropical cirrus help regulate the water vapor concentrations entering the lower stratosphere in the Tropics (Jensen et al. 1996; Hartmann 2002; Dessler and Sherwood 2000)

However, the processes that lead to the formation and maintenance of tropical cirrus are not well understood primarily because few measurements of their properties exist. In early 1987, the stratosphere–troposphere exchange project (STEP) was carried out in the vicinity of Darwin, Australia, to investigate the mechanisms controlling the formation and dissipation of cirrus anvils in connection with the observed extreme dryness of the stratosphere. A significant portion of tropical cirrus clouds was found to have optical depths greater than about 6 (Liou et al. 1990). Knollenberg et al. (1993) measured IWC of up to 0.07 g m^{-3} at temperatures ranging from $-60°$ to $-90°$C at the tops of tropical cumulonimbus. The Central Equatorial Pacific Experiment (CEPEX) offered in situ measurements of the ice crystal size and concentration, and particle habits. The results (McFarquhar and Heymsfield 1996) showed that the cirrus properties are closely related to the distance from the convective core where particles with larger cross-sectional area are found near cloud base and closer to the convection.

The Cirrus Regional Study of Tropical Anvil and Cirrus Layers-Florida Area Cirrus Experiment (CRYSTAL-FACE) field campaign held during July 2002 was designed to investigate the properties of convective systems and the resultant cirrus layers. With the exception of two flights into the Tropics on 9 and 26 July, the cirrus anvils studied were derived from convection forced by intense solar heating of the Florida Peninsula, so these cloud systems are not good surrogates for maritime tropical convection. However, the cloud condensation nuclei (CCN) measurements (VanReken et al. 2003) indicated that the aerosol sampled during the campaign was predominately marine in concentration. The observed convection and cirrus anvils had a much shorter lifetime, on the order of 3–5 h (Doelling et al. 2003), compared to that of tropical cirrus observed using trajectory analysis of satellite observations (Luo 2004). While field campaigns such as CRYSTAL-FACE are very useful, they tend to be limited in space and time, making it difficult to generalize our understanding of the cirrus formation, evolution, and dissipation processes.

Based on available observations and published reports, there appear to be two general classes of tropical cirrus (Pfister et al. 2001). One class appears to be related in some fashion to the detrainment of particles and water vapor from cumulonimbus clouds since it tends to exist in the layer where most penetrative convection reaches a level of neutral buoyancy in the Tropics. However, evidence exists that much of this cloudiness may form and be maintained through dynamical or radiative processes other than direct detrainment of water from deep convective towers (Pfister et al. 2001; Massie et al. 2002). Another class of cirrus exists in the stable regions of the TTL and, while it may be related to deep convection (Hartmann 2002; Dessler and Yang, 2003), it is likely not a direct outgrowth of the mass detrained from the convective clouds. Boehm and Verlinde (2000) find evidence that the TTL cirrus is related to vertically propagating Kelvin and gravity waves, while Pfister et al. (2001) argue that these clouds could be formed through synoptic-scale ascent along isentropic surfaces.

The cloud genesis is very important because it sheds light on the processes that produce and maintain cloud properties since it implies dynamical and meteorological information in the cloud-generating region. For example, thunderstorm anvil cases can involve strong updrafts in the convective core, which tends to modulate the characteristics of the particle size distributions that are detrained into cirrus layers according to modeling studies (Jensen et al. 1994). The fate of this anvil cirrus, especially for maritime clouds, is not well understood.

Pfister et al. (2001), using data from the Tropical Ozone Transport Experiments/Vortex Ozone Transport Experiment (TOTE/VOTE) campaign, analyzed isentropic trajectories and temperature histories and reported that the thin quasi-laminar cirrus and some of the thick clouds may be formed by in situ cooling and the thicker structured cirrus are more likely to be related to deep convection blow-off. They also reported that at most 25% of the west-central tropical Pacific has been directly influenced by convection within 10 days.

The distribution of tropical cirrus in relation to convection is also studied by Massie et al. (2002). By com-

bining the Halogen Occulation Experiment (HALOE) extinction for cirrus and aerosols and Climate Diagnostics Center outgoing longwave radiation data, they found that deep convection occupies only 7% of the equatorial region. Ninety percent of the cirrus clouds near the tropopause are located outside of deep convective regions. From the 5-day back isentropic trajectories calculated from ECMWF temperature and wind fields, they concluded that half of the HALOE cirrus observations over the Maritime Continent are consistent with formation by convective blow-off, while the other half are consistent with in situ formation processes.

There are some similarities between these two studies. First, both are focused on TTL cirrus, which underrepresents the total population of all tropical cirrus clouds. Second, long-term (5–10 days) isentropic trajectories and temperature histories are applied to find the cirrus relationship to deep convection. Consequently, these long-term tracking studies involve large regions of the Tropics, allowing them to examine cirrus properties over long space and time scales but opening them up to the inherent uncertainties associated with isentropic trajectory analysis.

In this paper we examine the origin and properties of non-TTL cirrus on shorter time and space scales than the Massie et al. (2002) or Pfister et al. (2001) studies by combining ground-based and satellite measurements. The questions we wish to address are whether, and to what extent, anvil cirrus evolve from detrained masses of ice crystals into entities that can maintain themselves through some set of dynamical and microphysical processes. The answers to these questions have implications for how tropical cirrus act to maintain the humidity structure of the tropical upper troposphere and the feedbacks these clouds have on the general circulation. Furthermore, from a practical standpoint, since the microphysical properties of self-maintaining cirrus are likely different from anvil layers, it is important to address how these clouds would be treated differently in remote sensing retrievals and in model parameterizations from young detrained anvil layers.

The ground-based data used in this study were collected by the U.S. Department of Energy (DOE) Atmospheric Radiation Measurement program (ARM) (Ackerman and Stokes 2003) from two observational facilities in the tropical west Pacific (TWP). One facility was implemented on Manus Island, Papua New Guinea (2.058°S, 147.425°E), in 1996 and the other on the island of Nauru (0.521°S, 166.916°E) in 1998. Manus is located within the heart of the Pacific warm pool where deep convection is frequent and widespread, while Nauru is located on the eastern edge of the warm pool where deep convection is much more episodic. The ARM program installed 35-GHz cloud radars (MMCR) (Moran et al. 1998) on their TWP facilities in 1998 (Nauru) and 1999 (Manus). To the ground-based ARM data we add the hourly Geosynchronous Meteorological Satellite (GMS) Lagrangian trajectories, derived from the technique described by Soden (1998), by which radiance patterns are followed for a 12-h period of time. These trajectories provide unique insights into the life cycle of cirrus observed at the two sites. With the back trajectories, we are able to follow cirrus from its point of observation over the ARM sites to either its source or until the back trajectory becomes unreliable (longer than 12 h).

The main issues we address in this paper are

1) the regional differences in the cirrus properties between the Manus and Nauru sites using MMCR observations,
2) the manner in which cirrus clouds at these two sites are related to deep convection within the previous 12 h using the millimeter radar data combined with the satellite-derived trajectories,
3) the sensitivity of the properties of the tropical anvil cirrus (in this paper, anvil cirrus refers to those layers that can be traced to deep convection within 12 h using back trajectories) to the temporal duration from their last association with deep convection,
4) the seasonal dependence of the cirrus properties observed at Manus.

The paper is organized in the following manner: section 2 compares the observed cirrus cloud properties between Manus and Nauru using one year of MMCR data. In section 3, the GMS satellite Lagrangian tracking data are introduced, and a satellite-based technique to detect the occurrence of deep convection in GMS IR imagery is discussed. The association of tropical cirrus with deep convection is examined in section 4, and finally in section 5, cirrus observed at Manus are grouped by season and studied in association with the properties of the regional convection using TRMM data. A summary is presented in section 6.

2. Millimeter-wavelength cloud radar observations

In this section we explore the characteristics of upper-tropospheric clouds observed at the tropical ARM sites with MMCR. The MMCR instruments (Moran et al. 1998) are key components of the observational suites at the ARM sites. They are zenith-pointing radars that operate at a frequency of 35 GHz and possess Doppler capabilities. Since the MMCR is able to

penetrate lower-level clouds and even light precipitation, the radar provides valuable information on cloud boundaries (e.g., cloud base, top). These radars are vertically pointing and have reasonable sensitivity to most cirrus below the TTL. The study of Comstock et al. (2002) showed that the MMCR has sufficient sensitivity to observe most cirrus that occur below approximately 15 km. Above 15 km, cirrus are often below the sensitivity threshold (~ -30 dBZ at this altitude) of the radar. Fifteen kilometers roughly marks the lower boundary of the TTL since most maritime tropical convection detrains below this altitude (Dessler 2002). The cloud physical temperature is obtained from regular radiosonde measurements (two per day) at the ARM sites.

As an active remote sensor, the MMCR transmits a pulse of millimeter-wave energy that propagates through the atmosphere until cloud droplets or precipitation reflects Doppler-shifted energy back to the MMCR receiver (Clothiaux et al. 1995). A digital signal processor records these signals and the integrated Doppler spectrum power or radar reflectivity (Z), mean Doppler velocity (V_d), and Doppler spectrum width (σ_d) are recorded. For solid spherical particles that are small with respect to the wavelength, the radar reflectivity, the zeroth moment of the Doppler spectrum, can be described as

$$Z = \int_0^\infty N(D) \times D^6 \, dD,$$

where N is the particle size distribution ($\mathrm{L}^{-1}\mu\mathrm{m}^{-1}$). It shows that the radar reflectivity is very sensitive to the largest particles in the size distribution. The Doppler spectrum is interpreted as a convolution of the Doppler velocity spectrum of the cloud particles with the probability density function of air motions (Gossard 1994). Since quiet-air particle terminal velocity positively depends on the ratio of mass to area (Mitchell et al. 1997; Heymsfield and Iaquinta 2000), the mean Doppler velocity, the first moment of the Doppler spectrum, also provides information on particle sizes and mass content (Mace et al. 2002). The spectrum width, the second moment of the Doppler spectrum, contains information related to both the turbulence and the dispersion of the particle size distribution.

Ice water content is another important property of cirrus clouds because it is closely related to ice water path (IWP) and optical depth, which determines the shortwave (solar) radiative transfer through the cloud layer. Liu and Illingworth (2000) analyzed published exponential relationships between IWC and radar reflectivity and reported that retrieved IWC from Z through a power-law relationship, which is classified in terms of temperature in 6-K steps, has bias less than 30%. In this study, IWP is calculated by integrating IWC in the cloud layer, which is derived from radar reflectivity using those temperature-classified coefficients.

One year of MMCR data (July 1999 to July 2000) are evaluated from both sites. We have found in our analysis of the Manus and Nauru MMCR data that a calibration error likely exists in the Manus data. In comparing the data from the two sites we found a systematic offset in the frequency distributions of various cloud classes for which we could find no reasonable physical explanation. Upon further investigation, we found the lower reflectivity limit reported in the data files of the Manus radar (i.e., the noise floor) was 6 dBZ lower than the noise floor of the MMCR at Nauru even though the radars are identical. In our subsequent analysis, we therefore add 6 dBZ to the radar reflectivity of the Manus radar. ARM instrument personnel concur that this correction to the Manus data is reasonable (M. Miller 2005, personal communication).

We define cirrus in this study as clouds observed by the MMCR with cloud base above 7 km. By examining eight months of MPL data between April and November 1999, Comstock et al. (2002) found that altocumulus clouds (i.e., clouds with enough liquid water to attenuate the micropulse lidar) above 7 km contribute less than 0.5% of all high clouds with base above 7 km at Nauru. We assume that Manus would have a similar distribution. During the period under study, the frequency of occurrence of clouds above 7 km observed by the MMCRs was 48% at Manus and 23% at Nauru. In Fig. 1, the cirrus cloud vertical frequency distributions at Manus (solid line) and Nauru (dotted line) are plotted. In Fig. 2 we plot several characteristics including the frequency distributions of layer-mean radar reflectivity, Doppler velocity, spectrum width, IWP (Liu and Illingworth 2000), temperature, and layer thickness for cirrus observed by the MMCR at Manus (dash line) and Nauru (solid line). The mean, mode, median, and standard deviation of these quantities are listed in Table 1 for the Manus and Nauru sites.

Overall, Fig. 2 suggests that the cirrus above Nauru are more tenuous with lower radar reflectivities, and smaller Doppler velocities, while the frequency distributions at Nauru are more peaked and have smaller variance than those above Manus. The radar reflectivity and cloud thickness of cirrus at Manus are skewed toward larger values, resulting in larger IWP overall. The spectrum width distributions are similar, while the Doppler velocity at Manus is larger than that at Nauru by 10 cm s^{-1}. The results are consistent with the cloud height distributions in Fig. 3. Even though cirrus at both

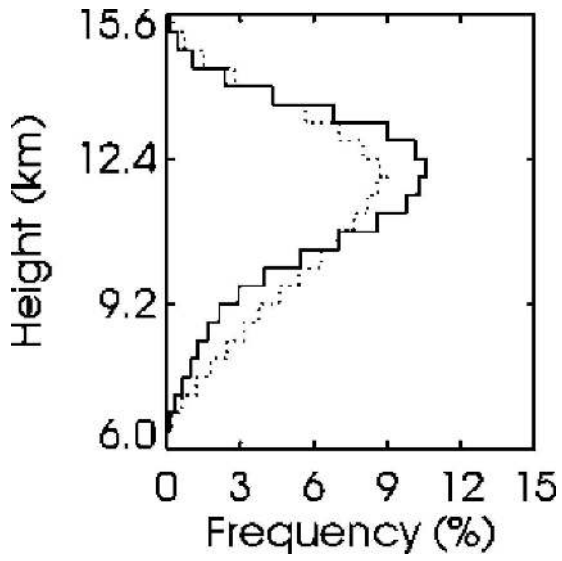

FIG. 1. The vertical frequency distribution of cirrus occurrence at Manus (dotted line) and Nauru (solid line). The frequencies shown are relative to the individual locations. Overall, the Manus MMCR reports cloud above 7 km 48% of the time during this 12-month period while at Nauru the frequency of occurrence is 23%.

sites have similar cloud-top-height distributions, at the Nauru site (solid line) the cirrus have a mean cloud base at 12 km, while the cirrus-base height at Manus (dotted line) peaks at 12 km but has an enhanced probability from 8 to 12 km. As indicated by Mather et al. (1998), this may be related to the stratiform regions of mesoscale convective systems.

The results summarized in Table 1 show that there are significant differences in the cloud properties observed at the two ARM sites. The significance of the differences are evaluated using a *t* distribution for testing the hypothesis that the distributions are drawn from the same sample, which we found to be untrue at the 95% confidence level. Generally, the cirrus at Manus are thicker and relatively warmer, with larger Doppler velocity, which suggests relatively larger mean particle sizes. Nauru is located in a region where deep convection is generally much more distant than Manus during non-ENSO periods. With this in mind, we explore the difference further by combining the MMCR radar and GMS satellite observations.

3. Geosynchronous Meteorological Satellite data and identification of deep convection occurrence

The GMS used in this study was located above the equator at 140°E and provided hourly observations of solar reflectance and emitted thermal radiation over the western tropical Pacific. The IR measurements used in this study have a horizontal resolution of 4 km and a thermal precision of 1-K brightness temperature.

Lagrangian trajectories of the cirrus observed by the MMCR are derived by applying the objective pattern tracking algorithm described by Soden (1998, 2004) to the GMS radiance measurements. The Lagrangian history of the cirrus observed by the MMCR is reconstructed by tracking the radiances from successive (hourly) water vapor images in a serial fashion backward in time. Starting from an initial target box of $2° \times 2°$ centered on the ARM site, the tracking algorithm searches for the highest spatial correlation between this radiance pattern and all possible matches 1 h prior ($t = -1$). If this pattern search is successful, the box at time $t = -1$ becomes the new target box and the algorithm searches for the highest spatial correlation between this pattern and all possible destinations at time ($t = -2$). A trajectory is then constructed by repeating this procedure through a 12-h period. Complete details regarding the tracking algorithm, its validation, and error characteristics are provided in Soden (1998, 2004). The Lagrangian trajectories calculated in this fashion are used to document the history of the cirrus clouds observed by the MMCR prior to their arrival at the ARM site. Using a technique to identify deep convection, described next, if the trajectory of the cirrus intersects a convective event, the time interval between the observation at the ARM site and the intersection is defined as the longevity or age of the cirrus observed at the ARM site.

The infrared radiances on geostationary satellites have been commonly used to identify convective clouds in tropical regions where other more reliable observations are sparse (Soden and Fu 1995; Inoue 1987; Steranka et al. 1984). There are three basic approaches to this problem. One method combines a fixed threshold in infrared brightness temperature (T_b) with a fixed threshold in visible reflectance. This method has the advantage that the reflectance provides valuable information about the column water content (Soden and Fu 1995). However, the visible data are restricted to daytime, while convective cloud formation over the tropical oceans has a maximum during night (Boer and Ramanathan 1997). Another technique (Inoue 1987) separates the optically thin clouds from thick clouds in day and night data using a fixed threshold in infrared brightness temperature and brightness temperature difference thresholds at two infrared wavelength bands. This technique is mainly used to detect cirrus clouds.

The cold cloud cover, defined by the area of the pixels with a brightness temperature lower than an arbi-

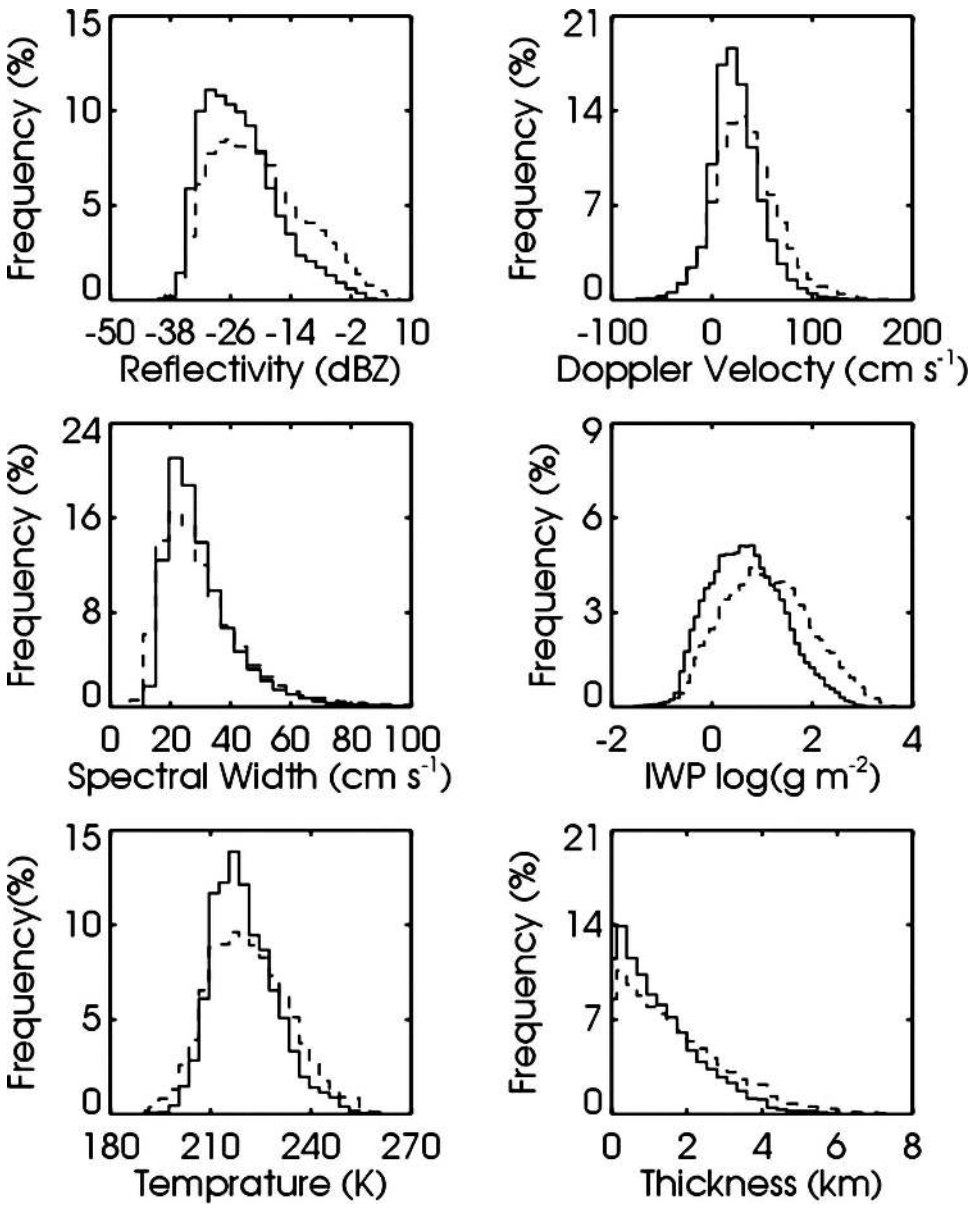

FIG. 2. The frequency distributions of radar reflectivity, Doppler velocity, spectrum width, IWP, temperature, and thickness of cirrus at Manus (dash) and Nauru (solid) from July 1999 to July 2000.

trary infrared threshold, is frequently used to estimate convective rainfall or occurrences of (mesoscale) convective complexes. This method assumes that the coldest area is associated with deep active convection. Steranka et al. (1984) investigated 23 tropical cyclones over the Atlantic Ocean and found that the mean cloud-top altitude of deep convection near the center of tropical storms is near 12 km, while that of the dense cloud canopy is about 9.7 km. These results showed the ability of this method to distinguish deep convection from their associated mesoscale anvils by choosing a sufficiently cold IR threshold. However, the collocated radar and infrared satellite observations (Adler et al. 1983; Zipser 1988) indicated that the coldest cloud tops were collocated with the overshooting of convective cells only at the beginning. Furthermore, as the convection propagated, weakened, and tilted with time, the areas of coldest cloud tops were observed to be progressively displaced from the convective region and more likely to be related to the formation of stratiform rain following the decay of deep convection.

To reliably identify the convective systems in satellite IR imagery, an optimized technique based on the single infrared threshold method is derived and evaluated us-

TABLE 1. The mean, median, mode, and standard deviation of cirrus cloud layer mean properties at Manus and Nauru (bold). Refer to Fig. 2.

	Mean	Median	Mode	Std dev
Radar reflectivity (dBZ)	−18.1	−19.4	−26.0	9.6
	−21.9	**−23.0**	**−30.1**	**7.7**
Doppler velocity (cm s^{-1})	45.3	43.1	30.0	34.0
	35.1	**32.9**	**20.0**	**27.2**
Spectrum width (cm s^{-1})	34.5	30.1	21.7	17.8
	33.4	**29.7**	**21.6**	**14.4**
Ice water path (g m^{-2})	38.4	7.7	7.0	103.9
	29.6	**5.7**	**6.3**	**86.0**
Temperature (K)	224.1	223.3	217.0	12.7
	222.7	**221.3**	**217.6**	**10.0**
Cloud thickness (km)	1.9	1.5	2.7	1.4
	1.5	**1.2**	**2.7**	**1.1**

ing radar measurements from the Tropical Ocean Global Atmosphere Coupled Ocean–Atmosphere Response Experiment (TOGA COARE) intensive observing period (IOP) combined with GMS satellite observations. From the four-month IOP period of TOGA COARE, 12 days (268 h) of 5-cm Massachusetts Institute of Technology (MIT) radar observations (DeMott and Rutledge 1998) collected onboard the R/V *Vickers* in the Intensive Flux Array (IFA) are selected as representative of the convective activity in this region. The area fraction of reflectivity and the maximum radar reflectivity at each level are used to describe the vertical structure characteristics of convection. To provide comparable data to our satellite tracking images, a region of $2° \times 2°$ (corresponding to a square of 200 km × 200 km in the equatorial regions) centered at the MIT radar is selected from the radar data and then collocated with satellite images. The radar base scan and IR image at 1742 UTC 30 January 1993 are shown in Fig. 4, where the radar reflectivity is plotted as the color image, while the IR temperatures (210 and 240 K) are shown as red contours. As expected, the coldest IR temperature areas (240 K) are located very close to the strong radar reflectivity (greater than 20 dBZ) areas.

Our radar deep convection detection definition is adapted from Szoke and Zipser (1986). An arbitrary reflectivity threshold (40 dBZ) at the surface is chosen to identify precipitation associated with deep convection. We require that at the surface the 20-dBZ area of radar echo is larger than 10 km^2 and the area of the 10-dBZ radar echoes at 10-km height is greater than about 5 km^2.

Figure 5 shows the evolution of convective events happening on 30 January 1993. The time–height cross sections of the area fraction of the $2° \times 2°$ box that has reflectivity of 20 dBZ or greater (i.e., the 20-dBZ area

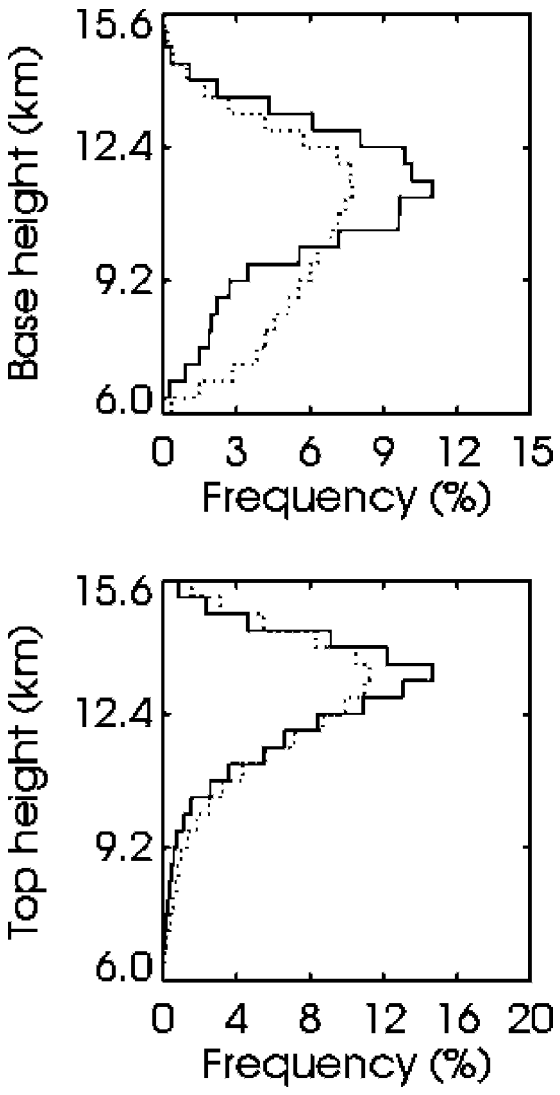

FIG. 3. The frequency distribution of cirrus cloud-base and -top height at Manus (dotted) and Nauru (solid).

fraction) and the maximum reflectivity suggest that there is a convective event decaying from 0300 to 0600 UTC. At about 1242 UTC, another convective event begins with a sudden increase of maximum reflectivity and 20-dBZ area fraction. From the satellite images, the area fractions of certain T_b thresholds and the minimum T_b are found and plotted in Fig. 5c. As we can see, the minimum T_b and the area fraction of all T_b thresholds decrease at the beginning as the first convection decays, and then begin to increase at 1330 UTC, which is about 1 hour later than the radar reflectivity response. As the second convective event begins to decay, the area fractions of each T_b threshold decreases again. The responses of radar reflectivity and the area fraction of each T_b threshold correspond very well with each

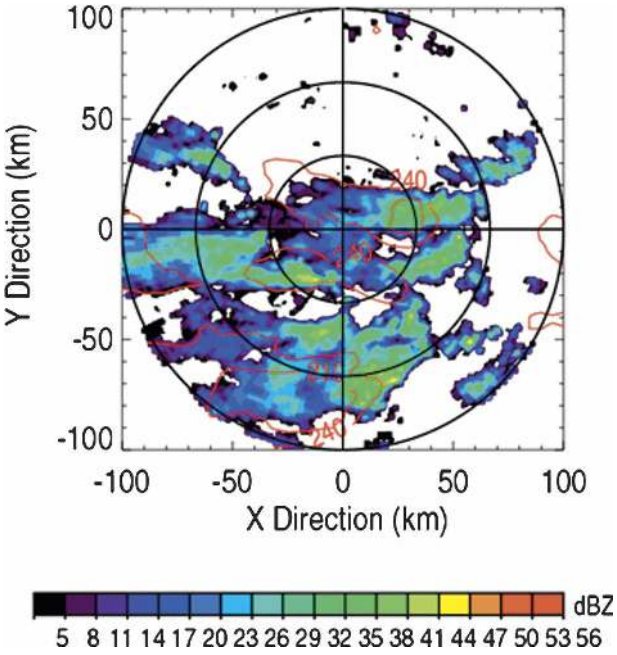

FIG. 4. A case study of a convective event on 30 Jan 1993 observed in the TOGA COARE intensive flux array by the MIT radar on the R/V *Vickers*. Shown are the radar base scan (color image) and IR brightness temperature (red contours) at 1742 UTC in the 2° × 2° region centered on the R/V *Vickers* radar. The IR temperature contours start at 210 K and progress in 10-K steps.

other except that the GMS observations have a 1–2-h lag, consistent with the time that anvils take to spread following the onset of deep convection.

Based on similar analyses as presented in Fig. 5, to identify deep convection in the GMS data, a candidate region must satisfy one of two possible criteria. Deep convection is considered to be occurring if at least one data pixel of 205 K or colder is identified. Less intense cases of deep convection may not reach such low temperatures, however. To include those less intensive convection cases, a minimum threshold of the 210-K to 240-K area ratio is then used since the stratiform clouds usually have a larger expanding cloud canopy with higher temperature than the parent convective towers. For the case on 30 January 1993, the radar method detected the convection from 1242 until 2142 UTC. However, the satellite criteria identified convection onset one hour later and continued the convection two hours longer than the radar method. From the 12 days (268 h) of MIT radar data from TOGA COARE, the statistical comparison showed that we had agreement between the radar-derived convection identification and satellite-derived definition 94% (253 h) of the time. In this period, 131 h are identified by both methods as having convection within the 2° × 2° box.

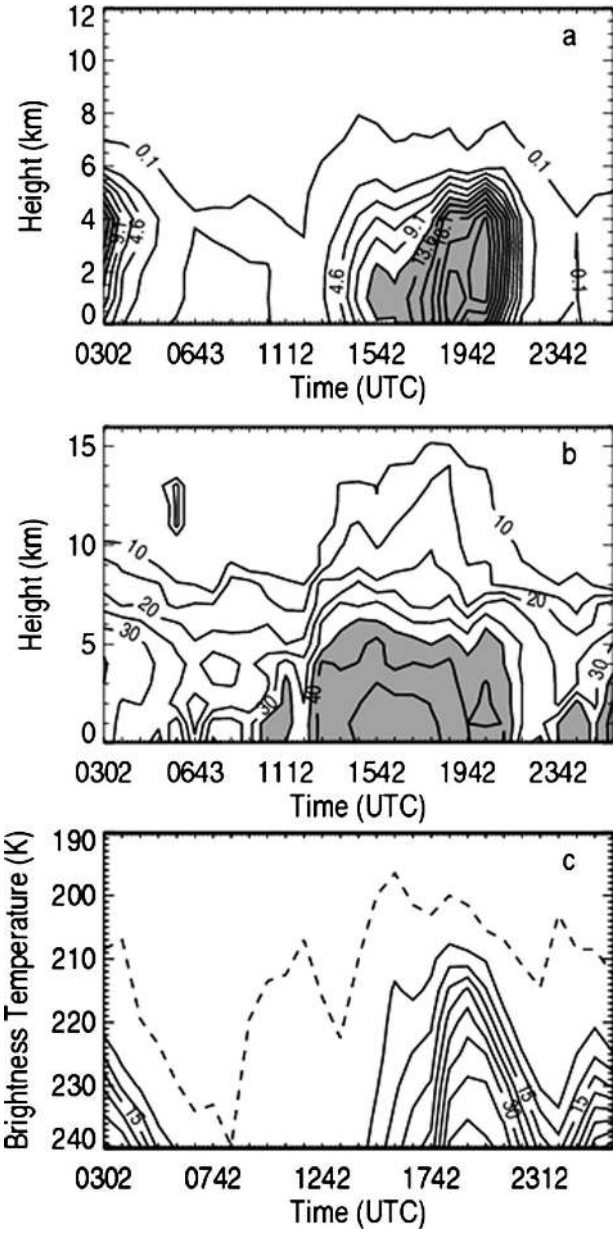

FIG. 5. Time series of radar reflectivity and satellite parameters from the convective event shown in Fig. 4. (a) The time–height plot of the 20-dBZ area fraction in the 2° × 2° region. (b) The time–height plot of maximum radar reflectivity in the region. (c) The time–T_b plot of area fraction. The minimum T_b is overplotted with a dash line.

4. Tropical cirrus association with deep convection

As an illustration of the technique used to examine the longevity-dependent properties of cirrus observed at the ARM sites, we present a case study of the time–height plot of MMCR radar reflectivity from 0000 to 1600 UTC 14 December 1999 (Fig. 6). The radar

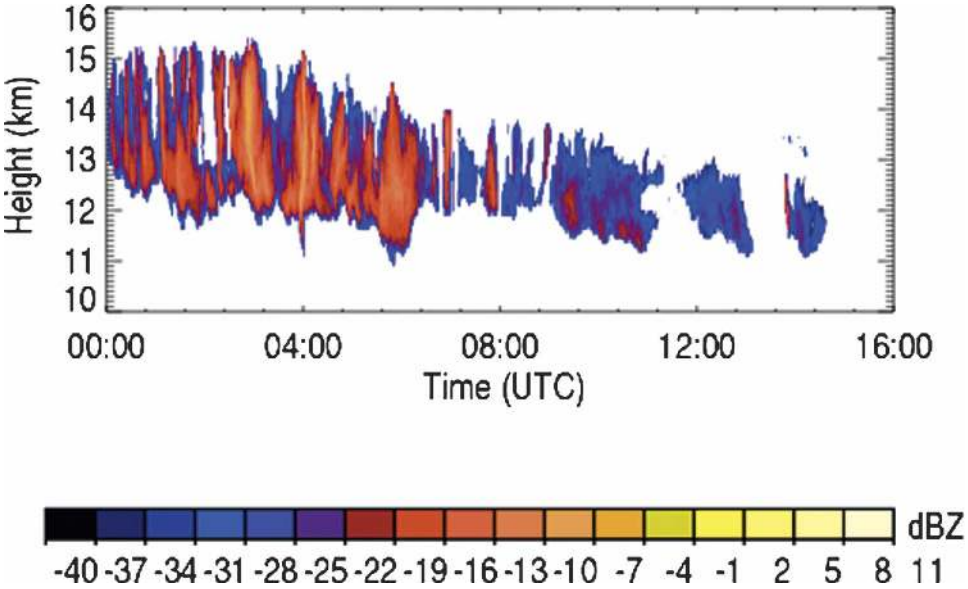

FIG. 6. Time–height plot of Nauru MMCR radar reflectivity recorded on 14 Dec 1999.

data show that for the first several hours of the event the cirrus layer had a top near 15 km and was getting thicker. During this period, the reflectivity was large and extended vertically with embedded fall streaks. The data suggest a high degree of temporal/spatial variability in the layer as it advected past the Nauru site (the upper-tropospheric wind during this period was from the northwest at about 10 m s^{-1}). After 5–6 h, the top of the layer began to descend while the bottom of the layer remained roughly constant. As the layer thinned, the reflectivity also decreased steadily until the layer was no longer detected by the radar. The Lagrangian tracking images provide the geographical track of the cirrus through the previous 12 h. Consider first the cirrus observed at 0200 UTC 14 December 1999. The large-scale GMS satellite images (12° × 12°) at t_0 (here t_0 is 0200 UTC 14 December 1999), $t_0 - 3$ h, $t_0 - 7$ h, and $t_0 - 9$ h are presented in Fig. 7. In each image of Fig. 7 the 2° × 2° satellite tracking box is delineated in white and the location of the Nauru ARM site is noted with a white dot. The center of these 2 × 2 regions denotes the most likely location of an upper-tropospheric air parcel traced back in time from the ARM site at t_0. As we can see from these satellite images, the cirrus observed at Nauru at 0200 UTC is traced along a northwesterly trajectory 9 h into the past to a huge convective complex. As a result, the cirrus profiles observed by the MMCR within this hour are estimated to be approximately 9 h old. The back trajectory of the cirrus observed at Nauru at 0200 UTC is plotted in Fig. 8.

As a further example, consider the cirrus observed at 0800 UTC 14 December 1999. This marks the approximate time when the cirrus began thinning (Fig. 6). Cirrus observed at this time was traced backward in time 12 h (Fig. 9) at which time the cirrus appear to have been detrained from a convective event to the northwest (Fig. 8). As before, the centers of these boxes represent the most likely back trajectory of the cirrus observed at 0800 UTC. On average, the cirrus observed at the Nauru site between 0000 and 0800 UTC 14 December 1999 originated from deep convection happening about 7 to 12 h prior (Fig. 10).

a. Cirrus longevity from its convection origin

In the year considered here (July 1999–July 2000), there are approximately 3672 h of cirrus observed at the Manus site, while at Nauru there are only about 2545 h of cirrus. Previous research (Mace and Benson-Troth 2002) also showed that more cirrus is observed at Manus than at Nauru. A data summary is listed in Table 2. Among these cirrus observations, 2334 and 1697 GMS Lagrangian trajectories are found for Manus and Nauru, respectively. From those trajectories, we find that 47% of the cirrus clouds observed at the Manus site can be traced to a deep convective event within the previous 12 h, whereas only ~16% of the cirrus at Nauru can be traced back to a convective event within the previous 12 h. Dividing the cirrus cases into five groups by ages (i.e., 0, 1–3, 4–6, 7–9, and 10–12 h), the frequency of cirrus at both sites are plotted as a function of age in Fig. 11. The tendency of these dis-

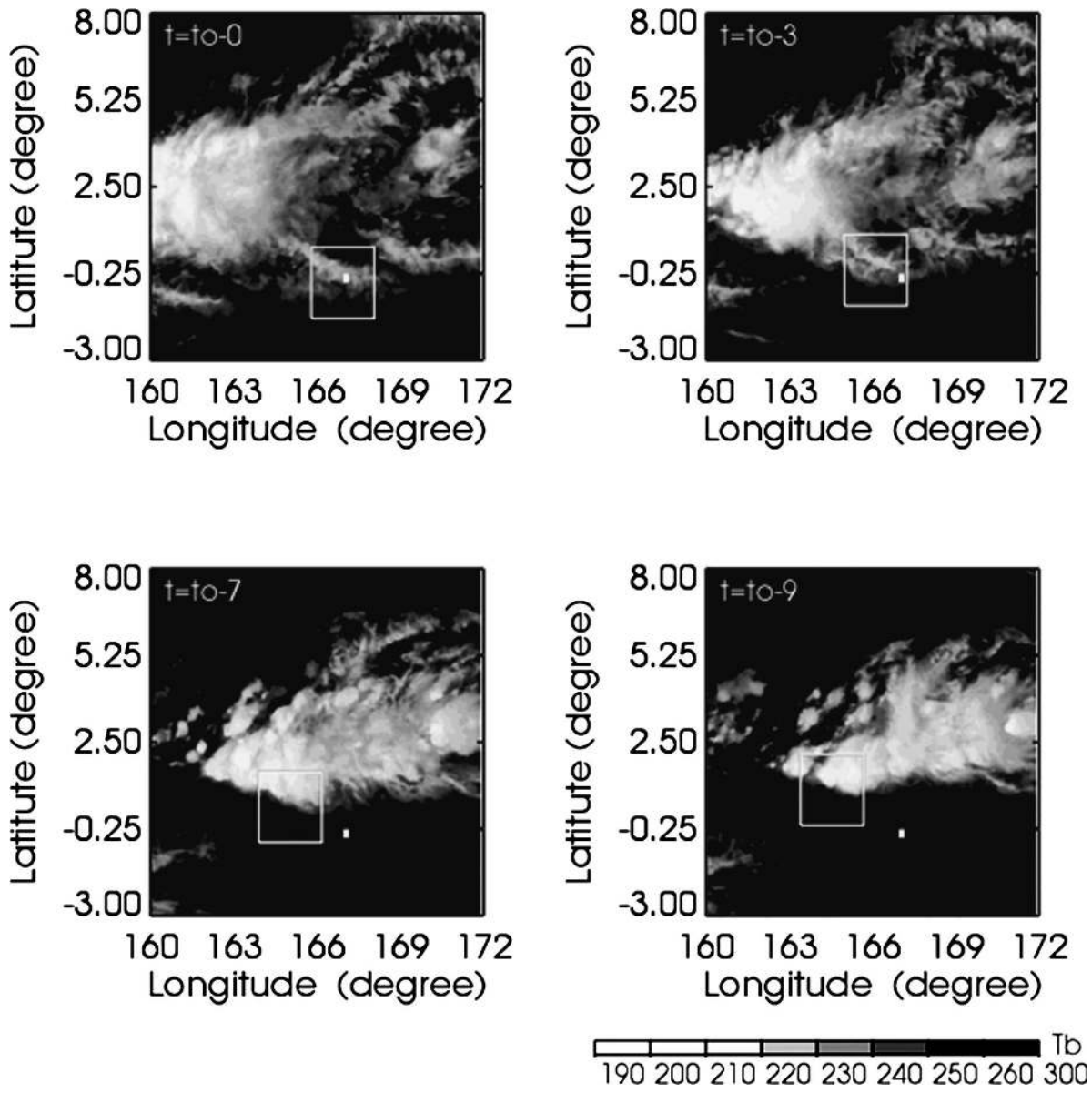

FIG. 7. The GMS large-scale images for cirrus clouds observed above Nauru at t_0 (0200 UTC 14 Dec 1999), $t_0 - 3$, $t_0 - 7$, and $t_0 - 9$. The white box is the location of the $2° \times 2°$ tracking images. The Nauru ARM site is noted with a white dot.

tributions at each site is clearly opposite one another with the frequency of cirrus decreasing at Manus as their age increases after the 1–3-h bin. In contrast, at Nauru the frequency of cirrus steadily increases as the age increases.

At Manus, about 50% of the cirrus that can be traced to deep convection are found to originate from a convective event within 3 hours of their observation by the MMCR, while for Nauru the percentage is only 20% during the period studied. The geographical proximity of the sites to the convectively active warm pool helps explain these findings. At 147°E, Manus Island was situated within a convectively active region during the La Niña that was influencing the western Pacific during the period under study. Nauru, at 166°E, was well to the east of the convectively active region. What is surprising about these results is that the cirrus at Nauru can maintain such extreme longevities and raises significant questions as to what processes maintain these clouds against the large-scale subsidence known to occur in the nonconvective regions of the Tropics (Sherwood 1996). This finding is also supported by Massie et al. (2002) who noted that much of the tenuous cirrus that they observed was located away from deep convection.

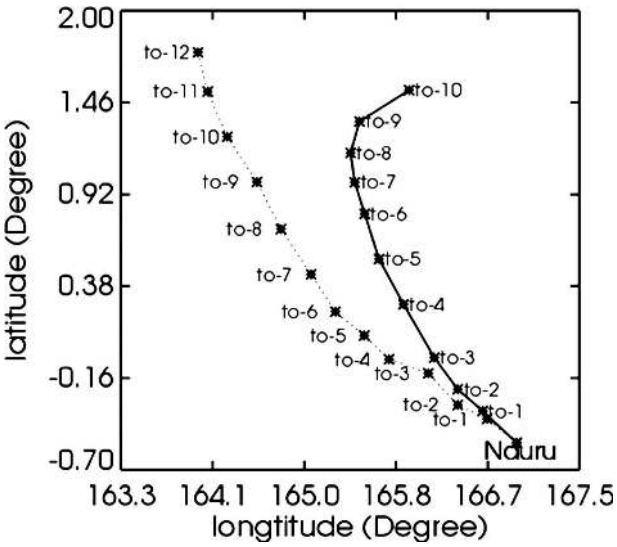

FIG. 8. The cirrus trajectory obtained from the center of the tracking images at 0200 (solid) and 0800 (dot) UTC 14 Dec 1999.

b. Anvil cirrus properties as a function of longevity

The evolution of anvil cirrus properties is a topic of considerable interest because the cloud microphysical properties influence the feedbacks that cirrus have on the climate system through radiative forcing and transport of water. To provide a more complete picture of the evolutionary process, we also consider the cirrus that did not track to deep convection within 12 h as a sixth classification with longevity (or age) longer than 12 h. Figure 12 shows the frequency distributions of the layer–mean millimeter radar reflectivity binned by dBZ_e and Doppler velocity for the six longevity classes at the Manus (dash) and Nauru (solid) sites. Here, 6 dBZ is added to the radar reflectivity factor observed at Manus because of the calibration offset noted above.

The frequency distributions are characterized by a bimodality of radar reflectivity and a unimodal distribution of Doppler velocity. The larger reflectivity mode has maximum frequency in the 1–3-h time bin and then decreases in predominance with time. The smaller reflectivity mode peaks near -25 dBZ_e for cirrus younger than 12 h and then shifts to -30 dBZ for cirrus that cannot be traced to deep convection. For the cirrus that cannot be traced to deep convection, the large reflectivity mode is not evident. The Doppler velocity probability distribution function migrates to smaller values as the large reflectivity mode decays. From the distributions of cirrus older than 12 h, it appears that two populations of cirrus exist in these datasets with a background population of relatively lower reflectivity and smaller Doppler velocity that has similar characteristics to the cirrus that cannot be traced to deep convection. The closer the cirrus are observed to the parent convection, the more numerous the cirrus that populate the large reflectivity mode with higher Doppler velocities. This mode appears to decay with a time scale of several hours.

The differences between the Nauru and Manus sites are intriguing. The cirrus statistics appear very similar to one another up through longevities of 4–6 h. Beyond this time, the large reflectivity mode at Manus seems to decay at a slower rate compared to the cirrus at Nauru. This remnant large reflectivity mode at Manus appears to result in a mean Doppler velocity that is higher by about 10 cm s^{-1}.

A time series of the averaged layer mean and standard deviation (vertical line) of the Doppler radar moments and IWP [derived from the Liu and Illingworth (2000) regression algorithm] as a function of age are plotted in Fig. 13. To calculate the layer-mean quantities, we average vertically and then create the average and standard deviation in each longevity bin from the layer averages (the average dBZ_e is derived by averaging Z_e). The radar moments and IWP at the Manus site decrease monotonically as the cirrus age increases. While at Nauru the mean value of radar reflectivity increases during the first 3 h; after that it decreases also. The layer-mean Doppler velocity and spectrum width at both sites generally decrease with increasing longevity. With the exception of the Nauru radar reflectivity and IWP time series in the smallest longevity bins; all of the trends are similar with site-dependent differences in details. The variance, while it decreases in an absolute sense for all quantities, remains about the same magnitude in a relative sense. For the IWP, the ratio of the mean and the variance is about 1, suggesting an exponentially distributed quantity whose exponential slope increases with time. In the quantities considered here, with the exception of the Doppler spectrum width, the magnitudes continue to decrease throughout the 12-h period. This suggests that the cirrus cloud systems have not reached a steady state (if they ever do) during the period that we are able to follow them.

The exception to this is the spectrum width. Since this quantity represents a convolution of the dispersion of the particle distribution and the turbulence, the fact that it reaches a steady state in the later longevity bins suggests that the turbulence associated with the anvil outflow has decreased by the 6-h time bin and/or that the variance of the size distribution has ceased to change significantly. It would seem that the former explanation is the most reasonable and that the nearly constant variance in the spectrum width beyond the 6-h bin represents the natural variability in the size distri-

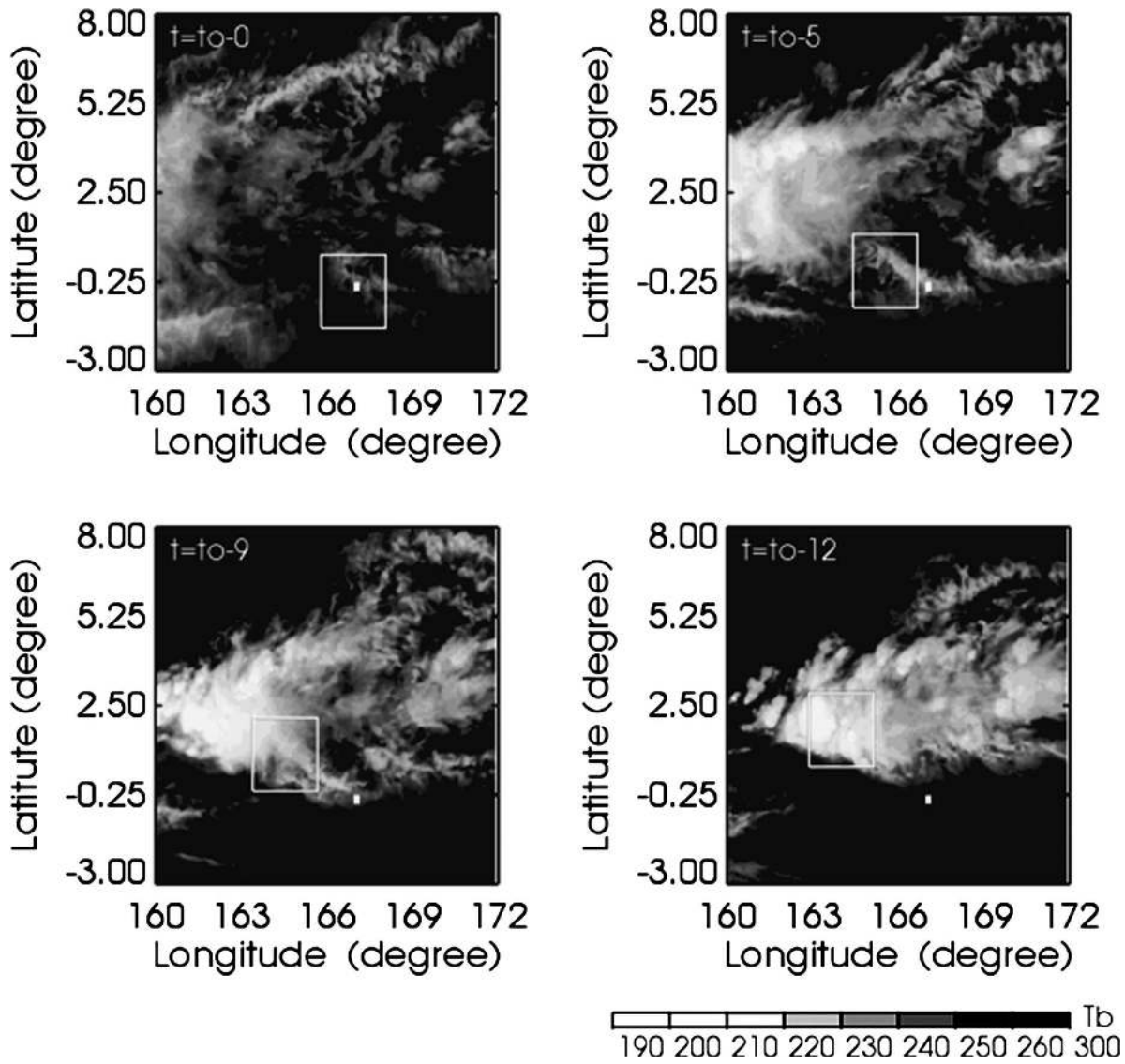

FIG. 9. The GMS large-scale images for cirrus clouds observed above Nauru at t_0 (0800 UTC 14 Dec 1999), $t_0 - 5$, $t_0 - 9$, and $t_0 - 12$. The white box is the location of the $2° \times 2°$ tracking images. The Nauru site is noted with a white dot.

bution dispersion beyond the time where the mean spectrum width ceases to change. Certainly more study and additional data will be required to confirm this speculation.

5. Seasonal variation of cirrus properties at Manus

With the exception of occurrence, and vertical distribution, it would seem that the cirrus properties observed by the MMCRs at Manus and Nauru as a function of age are similar to one another. Given the locations of the sites, it is somewhat surprising that the differences are not more pronounced. Manus Island, at 147°E, is in the middle of the equatorial warm pool region northeast of Papua New Guinea where deep convection is more numerous and cloud cover is more general than at Nauru located at 167°E on the edge of the warm pool where convection is rare especially during La Niña years, which 1999 was.

Using the trajectories that end with a convective event, a geographic frequency distribution of the convective origin of the cirrus is constructed for each site and plotted in Fig. 14. Manus tended to experience a greater frequency of events from the southeast, while at Nauru the convection in the southwestern quadrant contributed a significant fraction. Overall, the distribution at Nauru is more random for the relatively small number of events observed. Considering the cirrus lon-

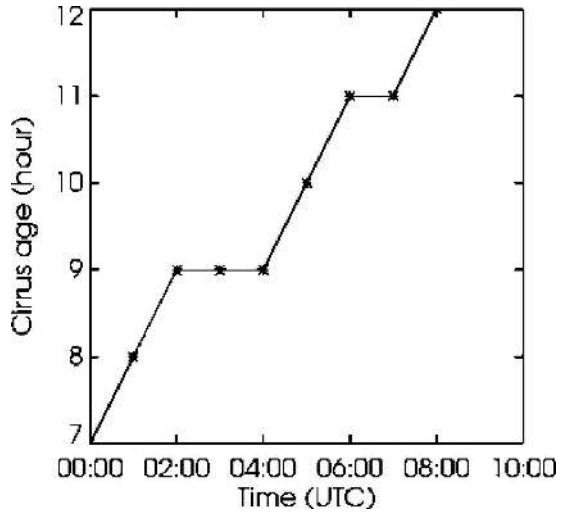

FIG. 10. The time series of estimated longevity for cirrus observed at Nauru on 14 Dec 1999.

gevity statistics presented earlier, about 50% of convection-associated cirrus observed at Manus originate from convection within 3 h of the observation time, while this statistic increases to 9 h at Nauru.

In the Manus region we find pronounced seasonal trends related to the migration of the intertropical convergence zone and the austral monsoon. During boreal summer (July–August 1999, July 2000, hereafter referred to as summer), the ITCZ migrates north of the equatorial region, while during boreal winter (January–April 2000, hereafter referred to as winter), convection is more pronounced over the large tropical islands in the Southern Hemisphere (Mather 2003). Given a predominantly easterly flow in the upper troposphere and the fact that few islands exist in the ocean region north and east of Manus, it is reasonable to examine whether the cirrus advecting over Manus during winter, when island-based or island-influenced convection is more pronounced, are different in some way from the cirrus observed during summer.

The trajectories of convection-associated cirrus at Manus in summer and the winter periods are plotted in Fig. 15. During winter, 90% of the trajectories (299) are from the southeast, originating from convection that is close to the islands of New Britain and Papua New Guinea (outlined with thick solid lines), while about 80% of those (269) in summer emanate from the northeast over open ocean. This suggests that the winter anvil cirrus observed at Manus have the potential to be more related to convection that has a greater degree of island influence, while the summer anvil cirrus derives from purely maritime convective sources. Recent results by Yeh and Chen (2002) have shown that offshore convergence due to the island topography effects would result in a coastal rainfall maximum. In the following we will consider whether and how the properties of cirrus and its convective origin observed at Manus during these two seasons are different from one another.

Figure 16 shows the 2D histograms of radar reflectivity and Doppler velocity of all anvil cirrus observed at Manus in summer and winter. Bimodality of the radar reflectivity–Doppler velocity joint PDF in winter is quite obvious. The histograms of layer-mean radar reflectivity and Doppler velocity of cirrus associated with deep convection are plotted as a function of age in Fig. 17. The anvil cirrus in winter (solid line) shows obvious bimodality in radar reflectivity in the age bins out through 12 h, even though the distribution narrows as

TABLE 2. Data summary of cirrus cases at the Manus and Nauru sites.

Sites	Cirrus observations (h)	Total trajectories available from GMS (h)	Trajectories that intersect deep convection (h)
Manus	3672	2334	1115 (47%)
Nauru	2545	1697	273 (16%)

TABLE 3. The mean and standard deviation of the retrieved cirrus cloud microphysical properties at Manus during summer and winter (bold) seasons, shown in Fig. 18.

	Mean	Standard deviation
IWC (g m^{-3})	0.0136/**0.0678**	0.356/**0.623**
Concentration (L^{-1})	105.53/**343.25**	730.9/**1169.7**
R_e (μm)	68.15/**61.31**	40.81/**35.76**
D_{mass} (μm)	414.07/**371.92**	247.7/**216.9**

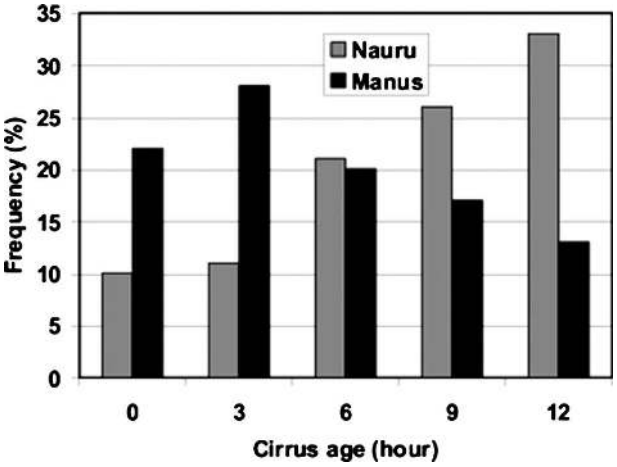

FIG. 11. The frequency distributions of anvil cirrus as a function of longevity at Manus (dark) and Nauru (gray), where these cirrus are associated with deep convection within 0, 1–3, 4–6, 7–9, and 10–12 h.

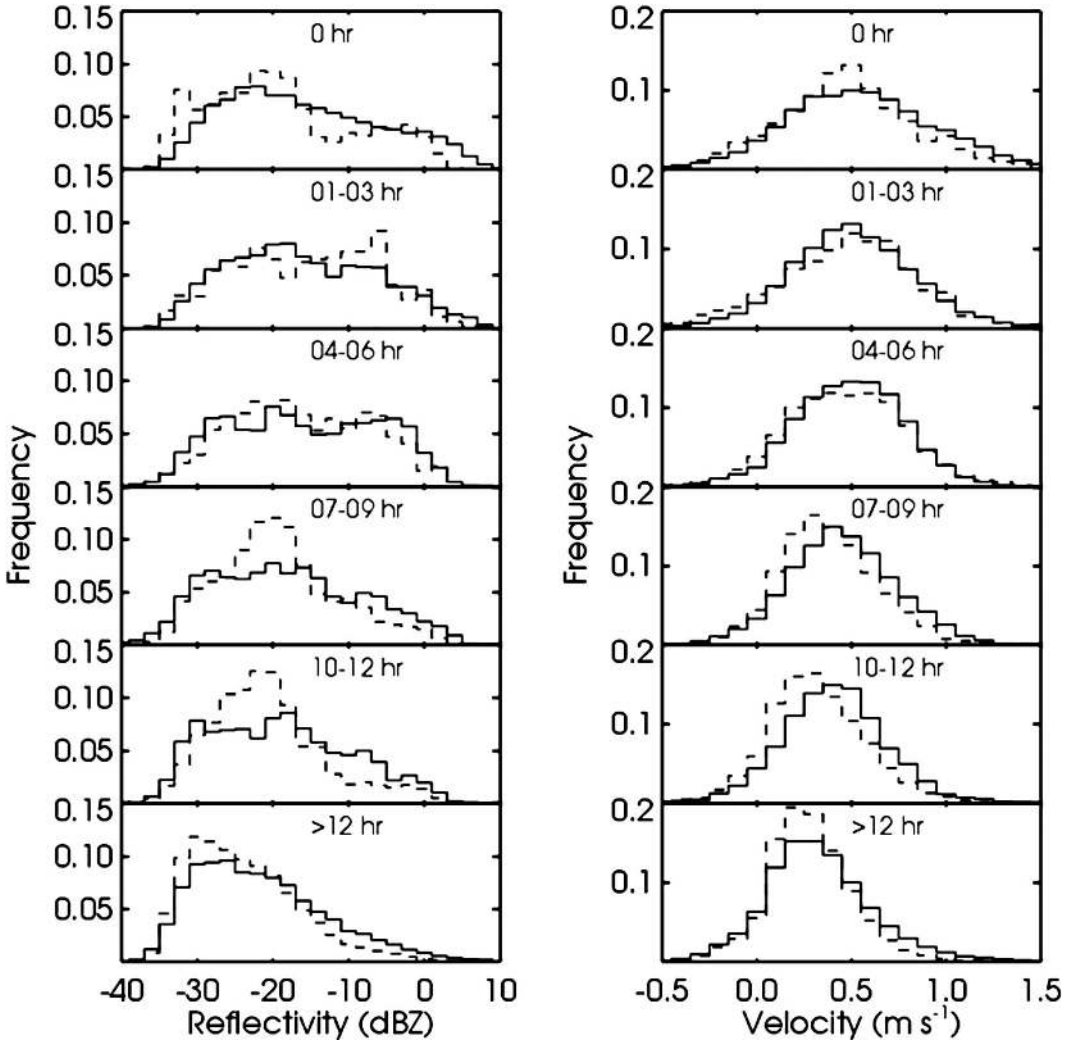

FIG. 12. The frequency distributions of (left) layer-mean radar reflectivity and (right) Doppler velocity in different longevity classes at Manus (dash) and Nauru (solid).

the age increases. Anvil cirrus layers from the summer period show a minimal large reflectivity mode and slight evolution of the reflectivity PDF with age. The summer maritime cirrus have smaller reflectivity overall than even the small reflectivity mode of the winter cirrus except for the classification with longevity longer than 12 h. The Doppler velocity distributions show subtle but important differences between these two seasons for longevities through 12 h. For ages less than or equal to 6 h, the Doppler velocity distributions are nearly indistinguishable from one another, yet the winter cirrus have a much higher radar reflectivity overall. We find a narrowing of the distributions with time and a shift of the mean values to smaller velocities. In the 7–9-h and 10–12-h bins, the winter cirrus Doppler velocity PDF shifts to smaller fall speeds, yet the reflectivity remains larger than in summer. For the cirrus that cannot be traced to deep convection, we find the reflectivity PDFs are indistinguishable from one another yet a significant difference is found in the Doppler velocity with winter cirrus having a smaller velocity overall. It appears that a residual difference exists in the cirrus even beyond 12 h, although it is impossible with this data to determine if the layers reach a steady state at some point beyond 12 h.

The microphysical properties can be mapped directly from a combination of the radar reflectivity and the Doppler velocity (Mace et al. 2002) assuming that the particle size distribution is exponential and that mean air motions are minimized. The microphysical properties such as particle concentration, effective radius, IWC, and mass mean size are retrieved and their distributions plotted in Fig. 18. The mean and standard deviation of these properties are listed in Table 3. We

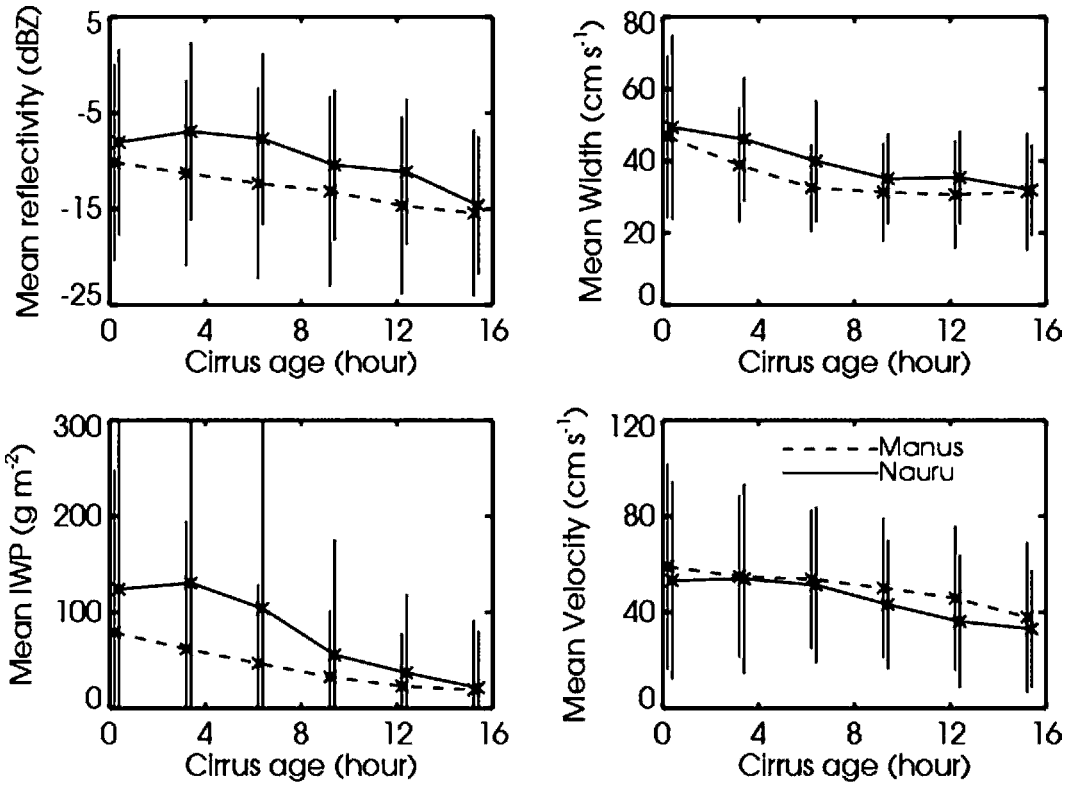

FIG. 13. The mean and standard deviation of radar observations and IWP as a function of longevity at Manus (dash) and Nauru (solid), where the cirrus clouds are divided into six classifications according to their estimated longevity. Here, all the cirrus that could not be traced to deep convection within a 12-h period following their observation are included in the 15-h longevity bin.

find substantial differences between the cirrus that pass over Manus during the respective seasons. Cirrus that arrive at Manus from convection to the southeast of the island tend to have much higher water content by about a factor of 10 due primarily to much higher particle concentrations of slightly smaller ice crystals. These differences follow directly from the differences in the radar reflectivity and Doppler velocity distributions plotted in Fig. 17. Recalling that most of the cirrus over Manus come from convection that is less than 6 h old, the similarities in the Doppler velocity distributions for cirrus younger than 6 h leads to nearly identical mean particle size PDFs. Because the reflectivity of these cirrus layers is larger than in summer, the only solution available to the retrieval algorithm to account for the higher reflectivity and similar Doppler velocity is for the particle concentrations to be much higher. The higher concentrations in turn lead to higher water content. While we do not show it here, if we were to plot the microphysical properties as a function of age, we would find that the cirrus older than 10 h are composed of smaller particles than similarly aged cirrus in summer with even higher relative concentrations.

The differences in the cirrus populations identified here could arise from a combination of sources. First, the parent convection could be different. It is well known that the dynamics and resulting microphysics of truly maritime convection is quite different from continentally driven convection. The extent to which the winter monsoonal cirrus could be considered continental is a matter of question, however, even though the convective origins of the anvils are closer to the large islands south of Manus than are the summer clouds. Additional evidence for this possibility is the fact that the Doppler velocity continues to decrease as longevity increases or the trajectories extend farther to the south and closer to the islands. The closer to the islands the trajectories extend, the smaller the particles and the higher the particle concentrations appear to be. The other source of difference could be in the dynamics of the upper troposphere that maintain the anvils once they are detrained from the convective towers. The nature of the differences in the vertical motion spectrum, the turbulence, and radiative forcing that would occur during these periods has not yet been investigated but could be very important to cirrus cloud evolution

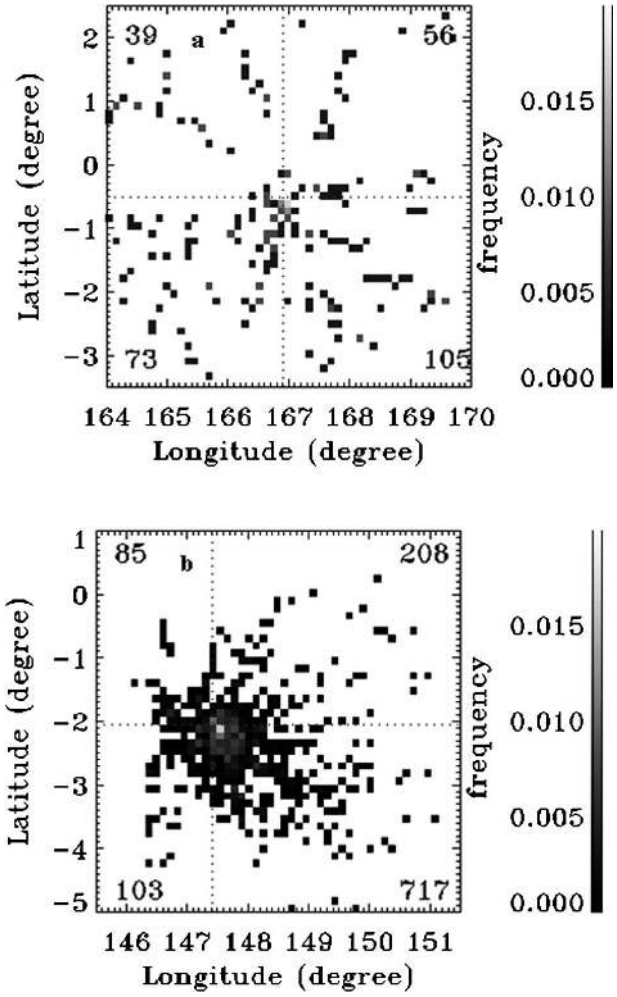

FIG. 14. The location distribution of deep convective origin of cirrus observed at (a) Nauru and (b) Manus. The number of total trajectories originating in each quadrant is noted within that quadrant.

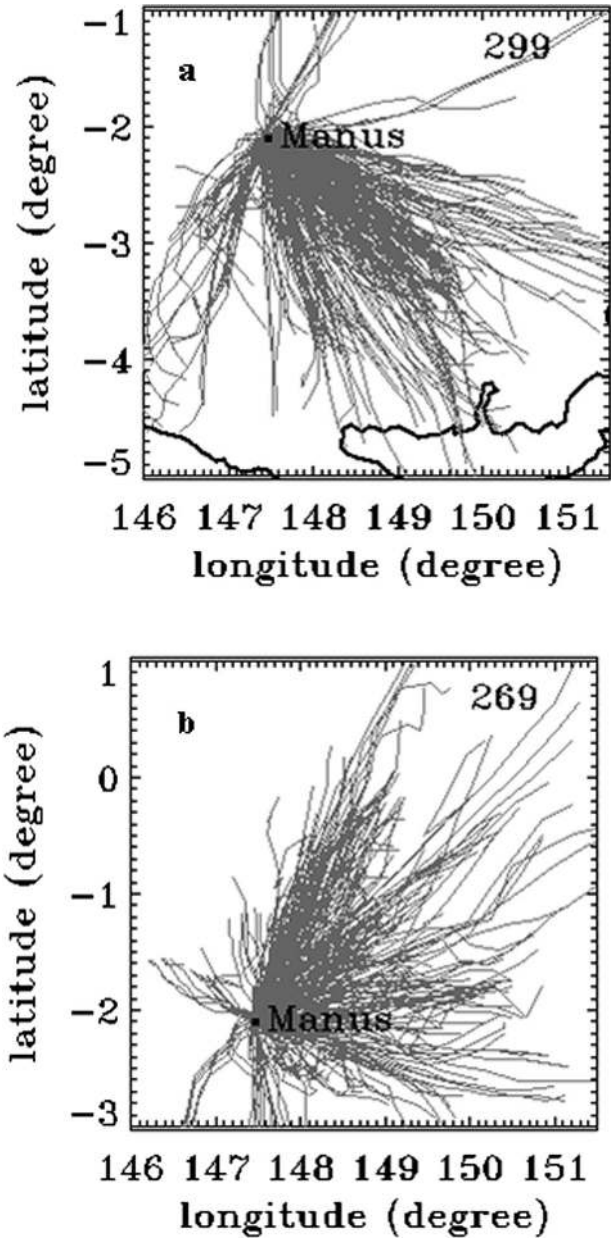

FIG. 15. The cirrus trajectories at Manus in (a) boreal winter/spring and (b) boreal summer. The number of total trajectories is noted in the upper-right corner.

(Boehm and Verlinde 2000; Ackerman et al. 1988). We attempt to address the former issue by examining statistics derived from the TRMM.

6. Evidence from TRMM for stronger convection south of Manus

The data from TRMM have been used for some time to characterize the intensity of convective cloud systems (e.g., Nesbitt et al. 2000; Petersen and Rutledge 2001; Toracinta et al. 2002; Cecil et al. 2005). The advantage of these data is that there are several independent proxies for convective intensity that are less indirect than IR brightness temperature (T_b). The precipitation radar (PR) measures vertical profiles of radar reflectivity with high accuracy and vertical resolution. The TRMM Microwave Imager (TMI) high-frequency channels (85 and 37 GHz) can be used to estimate precipitation ice water path. The lightning imaging sensor (LIS) can be used to detect flash rates above the detection limit of about 1 min^{-1}. A description of the instruments and their characteristics is found in Kummerow et al. (2000). One disadvantage of TRMM data is that the swath width and orbit conspire to limit the number of samples per month in any given location.

We use the algorithm of Nesbitt et al. (2000) to de-

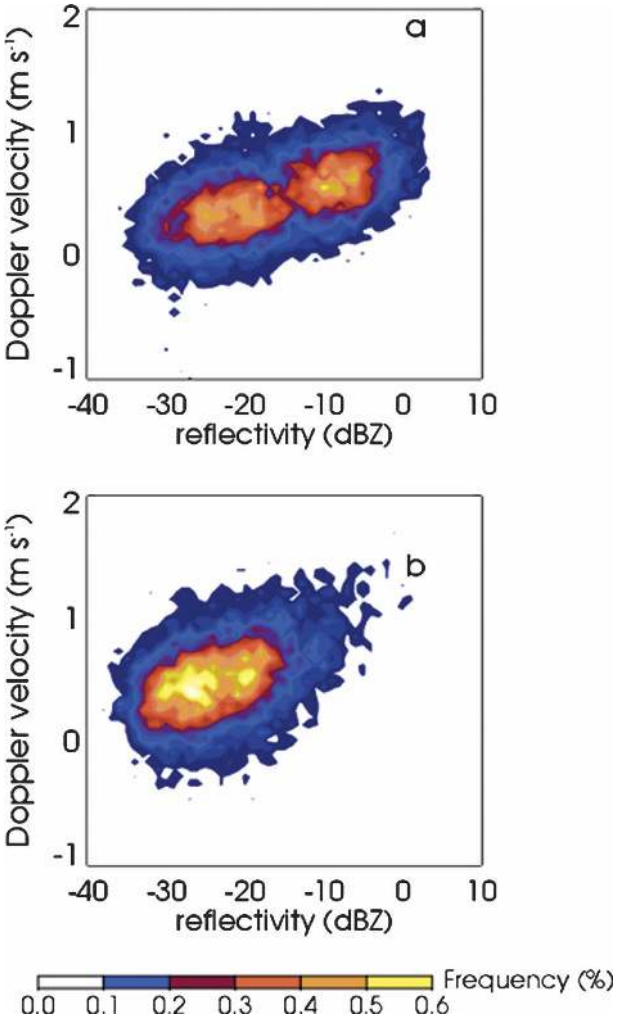

FIG. 16. The layer-mean radar reflectivity and Doppler velocity joint frequency distribution from anvil cirrus observed at Manus during boreal (a) winter and (b) summer.

fine contiguous precipitation features (PFs). The 85-GHz polarization-corrected temperature (PCT) is used for its convenience in distinguishing low brightness temperatures that result from attenuation of upwelling radiation due to heavy cloud ice in deep convection from low brightness temperatures resulting from low emissivity of the underlying surface. For the present purpose we consider only PFs with minimum $T_b < 250$ K, an effective discriminant that eliminates most weak or shallow features (Spencer et al. 1989), as we are seeking deep and vigorous convective systems capable of spreading anvil cirrus to Manus over a period of many hours. The lower the minimum T_b, the more ice scattering, the larger the ice water path, and presumably the stronger the convection. In convective cores, the use of PCT is justified, because minimum T_b is nearly identical whether horizontal or vertical polarization or PCT is used.

Our original intent was to use the same size boxes (2°) for analysis of the TRMM data as we used for the IR data. However, the sample size for strong PFs was quite small, so we expanded the boxes to 4° squares with Manus situated on the southwest corner of the summer box and on the northwest corner of the winter box (Fig. 20), and used our full 5-yr TRMM database, eliminating only the January–April 1998 period, which was possibly unrepresentative owing to the strong warm ENSO at that time. There were no significant differences in the limited statistics from the small box compared with the larger time–space domain.

Table 4 illustrates that by most criteria shown (and most not shown) there is a small but consistent difference between the summer and winter seasons. Even though the absolute difference in each quantity is small, there is a significant difference in convection intensity between these two seasons in the respective boxes containing most of the trajectories. In June–August (JJA), when oceanic cirrus observed over Manus emanates primarily from the northern box, proxies for convective intensity are weaker than those from the southern box in winter. The differences between the medians are small. Only when the stronger events (top 20%) in each box are compared do the differences become larger and make a clearer impression. The 85-GHz difference in minimum T_b increases from 1.6° to 15°C, and the maximum radar reflectivity at $z = 9$ km increases from 0.5 to 2.2 dBZ. While some of the differences are quite small, they are each partially independent measures and all act in the same sense.

Histograms of the various proxies for convective intensity (Fig. 19) demonstrate the tendency for the differences between the summer and winter seasons to be principally in the frequency of the stronger events. Convective cloud-top heights differ only slightly, probably signifying that even weak oceanic convection often approaches the tropical tropopause. But stronger updrafts will loft larger ice particles higher in the storm, increasing the radar reflectivity in the upper troposphere, the larger ice water path gives lower microwave T_b, and a greater probability of lightning (Zipser and Lutz 1994; Boccippio et al. 2000; Petersen and Rutledge 2001; Toracinta et al. 2002; Williams et al. 2002). The south box in January–April (JFMA) shows a small but convincingly greater incidence of lightning, storms with 85-GHz PCT < 150 K, and higher radar reflectivities in the ice region. The question remains whether this is a direct result of proximity to land, notably the large islands of New Guinea and New Britain, or also charac-

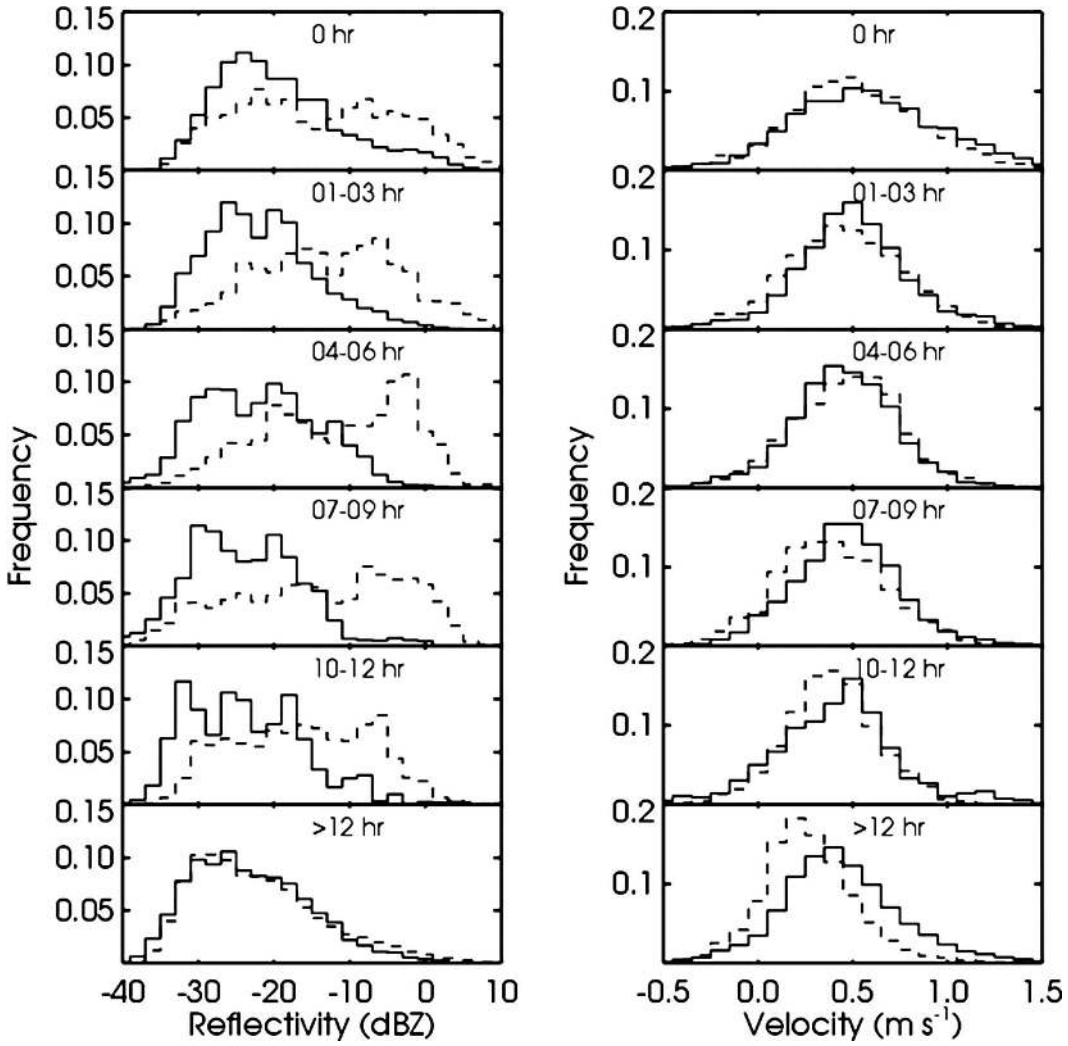

FIG. 17. As in Fig. 12, except that the dash and solid lines stand for anvil cirrus observed in summer and winter/spring at Manus, respectively.

teristic of the open ocean areas. Our analysis indicates that it is a combination of both.

Following the scheme of Cecil et al. (2005), Fig. 20 is a color-coded example of the data used to derive the distributions in Fig. 19. Each precipitation feature is located on the map, with progressively more rare and more intense measures shown by small black dot–green dot–orange diamond–purple asterisk–black triangle. The scale is calibrated against relative frequency over the entire tropical oceans for the 5-yr database. For example, orange symbols are centroids of PFs where the maximum height of the 20-dBZ contour reaches between 16.2 and 17.7 km. The southern box in JFMA has a few more of them, but the point of the map is to also show that the entire oceanic belt between 5° and 10°S has more of them than the JJA map does in the zone to the north of Manus. It also demonstrates that there is a greater concentration of strong events close to New Guinea and New Britain, so some, but by no means all, of the greater number of strong convective events near Manus in JFMA can be attributed to proximity to islands. We have also looked at the events over the land areas (not shown) and they are neither frequent enough nor strong enough to alter these conclusions.

While further study is needed, it appears that the TRMM data corroborate the findings from the Manus MMCR data. The cirrus that advect over Manus during the winter season originate from convection that is more intense more frequently, and the detrained anvils from these intense events likely have higher concentrations of smaller particles. This winter convection generates a population of particles in the extended anvils and cirrus that have a distinct bimodal distribution of

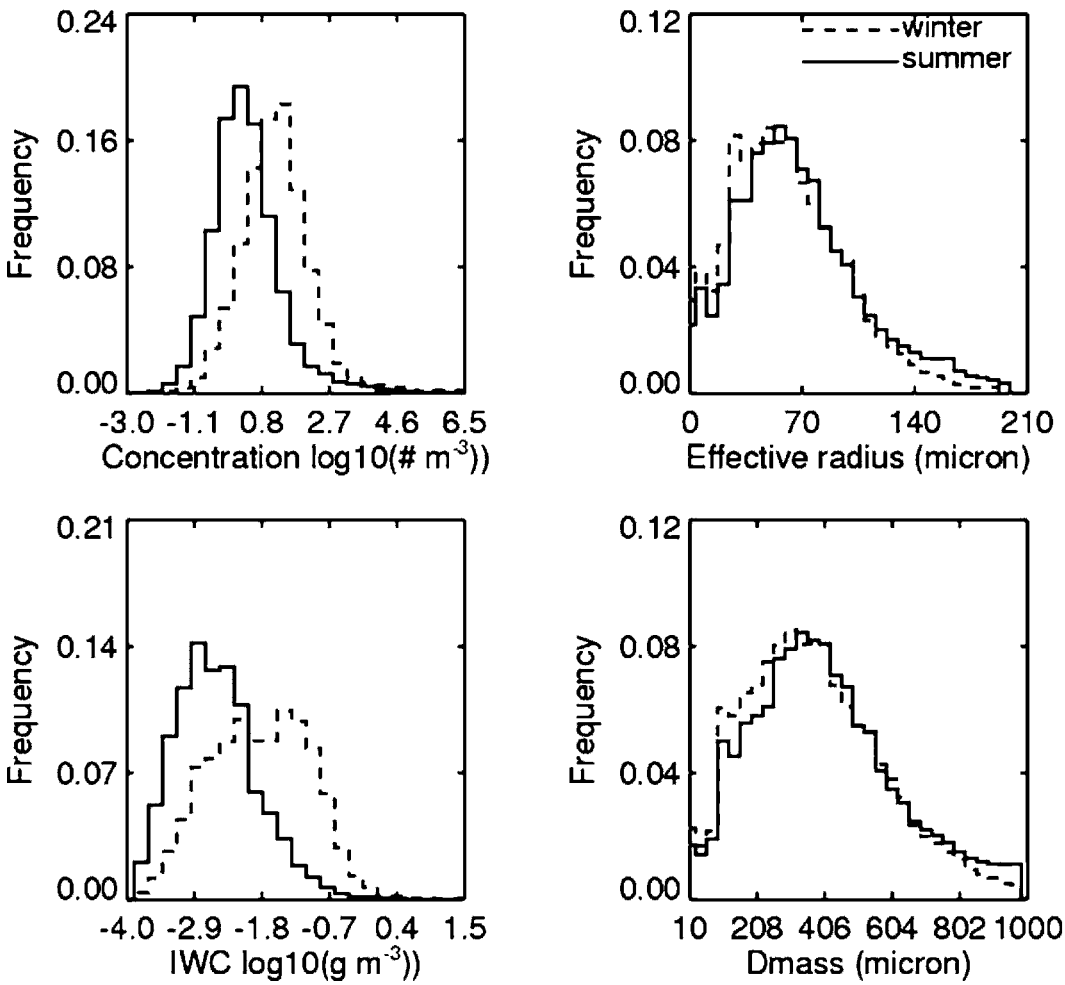

FIG. 18. The microphysical properties of cirrus observed at Manus during boreal winter/spring (dash) and summer (solid) mapped from Fig. 17 using a cloud property retrieval algorithm that relies on radar reflectivity and Doppler velocity (Mace et al. 2002).

radar reflectivity as measured by the MMCR with an overall smaller Doppler velocity in the small reflectivity mode compared to the summer cirrus. This difference is most notable when the properties of the clouds as a function of longevity are considered, and the TRMM data indicate that these differences are not confined to a limited area. These winter monsoon cloud layers are characterized by higher concentrations of small par-

TABLE 4. Properties of precipitation features (PFs) from TRMM. Sample size: 504 PFs in JJA, 563 PFs in JFMA. Box locations: JJA: north of Manus (2°S–2°N, 147°– 51°E), JFMA: south of Manus (2°–6°S, 147°–151°E). Months included: JJA1998–2000, 2002–2003; JFMA 1999–2000, 2002–2003.

Months	Min 85-GHz PCT (K)	Max height 20-dBZ echo (km)	Max echo at 6 km (dBZ)	Max echo at 9 km (dBZ)	Average rain rate (mm h^{-1})	PF area (km^2)
		(a) Median properties of PFs in 4° × 4° latitude–longitude boxes				
JJA	227.9	9.50	32.5	21.4	3.5	806
JFMA	226.3	10.00	33.0	21.9	3.6	977
		(b) Mean of top 20% in each category in the same boxes				
JJA	148.6	14.01	43.7	32.6	6.9	30 010
JFMA	133.3	14.38	44.5	34.8	8.3	31 620

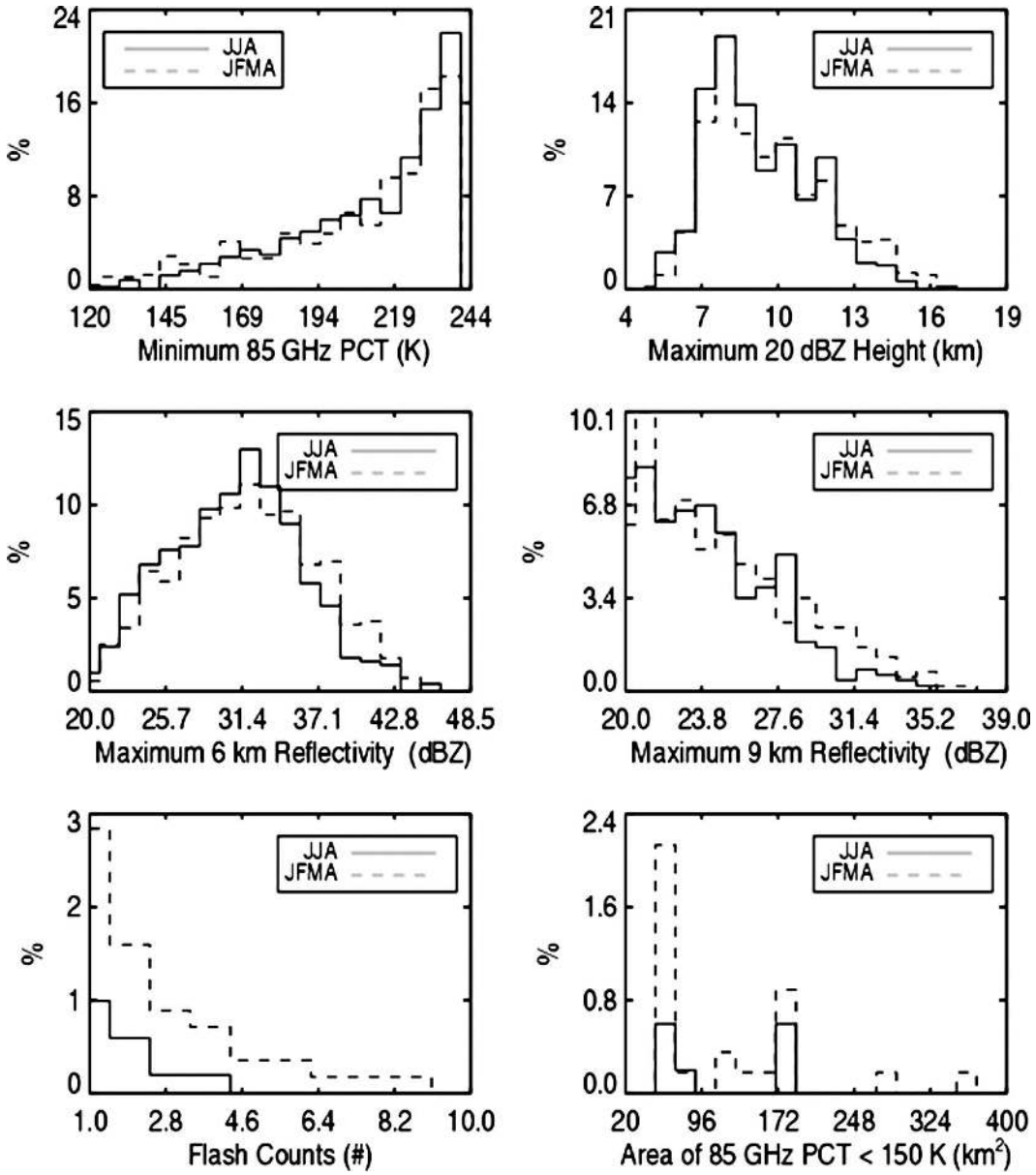

FIG. 19. Relative frequencies of occurrence of convective intensity proxy indicator magnitudes for precipitation features in the TRMM database within 4° × 4° boxes noted in Fig. 20. Table 4 provides additional information. The box north of Manus is used in June–August; south of Manus in January–April.

ticles compared to the summer season cirrus that advect over the MMCR from relatively weaker maritime convection.

7. Summary and conclusions

Because they exert such a significant control on the energy budget of the atmosphere, tropical cirrus clouds represent an important yet poorly documented component of the global climate system. In this study, we compare the properties of cirrus cloud layers that were observed at the Manus and Nauru ARM sites by vertically pointing millimeter-wavelength cloud radars (MMCR). The cirrus that we examine are found to populate the layer in which the majority of deep convection in the Tropics finds its level of neutral buoyancy—namely, the 10–15-km altitude range. This cirrus is distinct from the thin tropopause transition layer cirrus examined by other researchers (Pfister et al. 2001; Massie et al. 2002). By combining the MMCR data collected over a 1-yr period with GMS satellite-derived

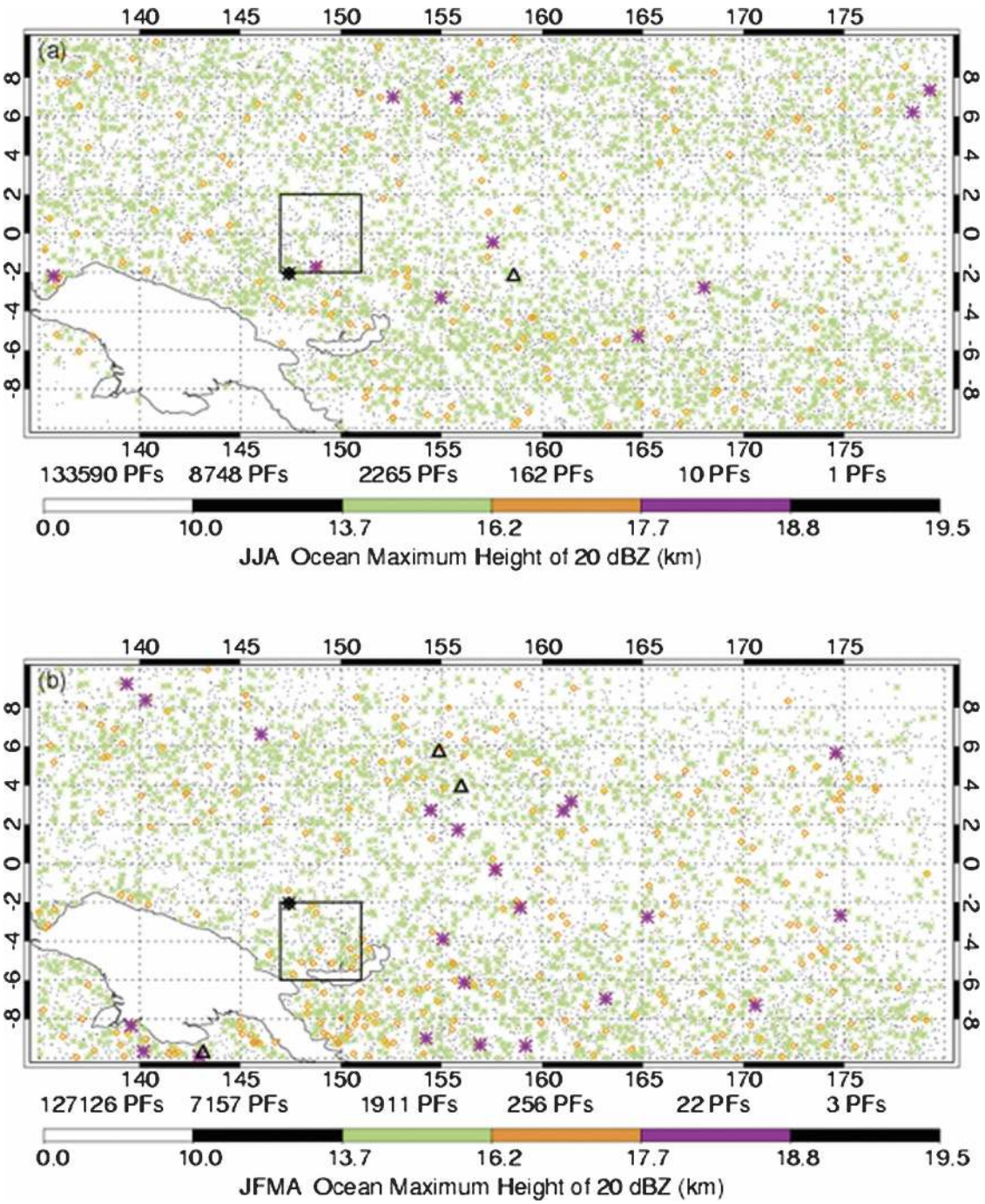

FIG. 20. Distribution of PFs in the TRMM database over the tropical western Pacific region. The 4° × 4° boxes used for each season are shown; the black asterisk locates the Manus MMCR site. The color code shows the maximum height reached by the 20-dBZ contour for each PF, progressing from small black dot–green dot–orange diamond–purple asterisk–black triangle for increasingly rare and intense PFs (see text).

trajectories (Soden 1998), we examine 1) the association of cirrus with deep convection, 2) how the cirrus layers evolve with time, and 3) how the cloud properties vary as a function of geography and season.

We find that cirrus at Manus tend to occur more frequently, are thicker, and therefore warmer on average than at Nauru. The frequency distributions of radar Doppler moments, corrected for an apparent calibra-

tion error at Manus, also show differences with overall larger radar reflectivity and Doppler velocity at Manus, while the cirrus at Nauru appear to be more uniform with less variability than the cirrus over Manus. Given the geographical locations of the ARM sites, these findings are not surprising.

To further explore these differences, we examined the association of the observed cirrus with deep convection by combining the MMCR observations with trajectories derived from GMS data. The 12-h satellite back trajectories allowed us to explore the cirrus history and hence helped us to investigate their association with deep convection. From the one-year dataset, we found that less than half of the observed cirrus at the ARM sites can be traced to deep convection within a 12-h period. Cirrus at Manus are associated with deep convection more often (47% of all cirrus observed) than at Nauru (16%). These results are significant because they suggest that cirrus in the Tropics must evolve in some way from detrained anvils into entities that are maintained by some other dynamical process (i.e., Lilly 1988; Sherwood 1996) that allows the layers to persist for extended periods of time. Consider that an ice crystal with a terminal velocity of 20 cm s^{-1} (a low rough average from the MMCR) would take just 6 h to descend 5 km through the layer of peak cirrus occurrence and 12 h to fall from 15 km to the freezing level.

The cirrus properties show a distinct evolution with layer age from a deep convective origin. The radar moments and IWP of the cirrus at both sites generally vary in a remarkably similar way (Figs. 13 and 14). The young anvil cirrus tend to have a bimodal distribution of radar reflectivity and broad PDFs of Doppler velocity and Doppler spectrum width. As the anvils age, the bimodal structure of the reflectivity PDF evolves into a more unimodal distribution as the large reflectivity mode decays. As this occurs, the velocity and spectrum width PDFs narrow and migrate to lower values. This evolution continues through 12 h for the reflectivity and Doppler velocity. However, the spectrum width reaches a minimum at 6 h, implying perhaps that the turbulence associated with the initial detrainment (Lilly 1988) has smoothed to a background level. It may also be the case that the signal processing of the radar observations is unable to resolve further decrease in the spectrum width.

The temporal evolution of cirrus also seems to be sensitive to the properties of the parent deep convection. We divide the trajectories by season at Manus where, during boreal winter, the trajectories emanate from convection that occurs to the south and east of the island, while during boreal summer the trajectories originate in the maritime regions north and east of the island. We found distinct differences between these populations with winter cirrus having overall higher water contents and also higher concentrations of small particles compared to the summer season maritime cirrus. These findings are consistent with TRMM data that show evidence for a higher frequency of more intense convection south and east of Manus during the winter monsoon compared to summer. The TRMM data also indicate that the stronger convection to the south is partly influenced by the proximity to large islands, but that this stronger winter monsoon convection extends far to the east as well. While the causes of these differences are unknown at this time, we can conclude that, if we are to understand and model the effect of tropical cirrus on the radiation and water budgets in the Tropics, both the nature of the parent deep convection and the dynamical maintenance of the cirrus layers must be correctly accounted for.

Although this research provides some limited insight into the nature and evolution of tropical cirrus in relation to deep convection, this study is compiled from observations collected during a fairly short period of time during the waning months of a strong La Niña episode. By considering the data as a statistical entity, we are making an implicit assumption that the dataset represents a statistically stationary snapshot of tropical cirrus and that, by categorizing the cirrus based on longevity, we can gain information on the evolution of these clouds during their existence. If the processes, presumably driven by the very largest dynamical scales, were changing with time over the entire basin, then our implicit assumptions may not be valid. Therefore, consideration of additional years of data will be required to confirm these results. Beyond simply examining more data, these observational results should be combined with process modeling of tropical cirrus evolution. Exploiting the synergy of observations and cloud-scale modeling is essential if our understanding of the processes leading to the observed evolution of tropical cirrus is to be improved so that parameterizations in climate models can eventually be considered realistic.

Acknowledgments. This research has been supported by the Environmental Science Division of the U.S. Department of Energy (Grants DE-FG0398ER62571 and DE-FG02-05ER64035). Data were obtained from the Atmospheric Radiation Measurement Program sponsored by the U.S. Department of Energy, Office of Science, Office of Biological and Environmental Research, Environmental Science Division. Analysis of the TRMM data was supported by the NASA TRMM Office under grant NAG5-136280682. TRMM data assistance was provided by Yaping Li and especially

Chuntao Liu. We gratefully acknowledge many insightful conversations with Dr. Steve Krueger during the early phases of this research. Paul F. Hein assisted generously in the acquisition and interpretation of the MIT radar data.

REFERENCES

Ackerman, T. P., and G. Stokes, 2003: The atmospheric radiation measurement program. *Phys. Today,* **56,** 38–45.

——, K.-N, Liou, F. P. J. Valero, and L. Pfister, 1988: Heating rates in tropical anvils. *J. Atmos. Sci.,* **45,** 1606–1623.

Adler, R. F., M. J. Markus, G. Szejwach, W. E. Shenk, and D. D. Fenn, 1983: Thunderstorm top structure observed by aircraft over flights with an infrared radiometer. *J. Climate Appl. Meteor.,* **22,** 579–593.

Boccippio, D. J., S. J. Goodman, and S. Heckman, 2000: Regional differences in tropical lightning observations. *J. Appl. Meteor.,* **39,** 2231–2248.

Boehm, M. T., and J. Verlinde, 2000: Stratospheric influence on upper tropospheric tropical cirrus. *Geophys. Res. Lett.,* **27,** 3209–3212.

Boer, E. R., and V. Ramanathan, 1997: Lagrangian approach for deriving cloud characteristics from satellite observations and its implications to cloud parameterization. *J. Geophys. Res.,* **102,** 21 383–21 399.

Cecil, D. J., S. J. Goodman, D. J. Boccippio, E. J. Zipser, and S. W. Nesbitt, 2005: Three years of TRMM precipitation features. Part 1: Radar, radiometric, and lightning characteristics. *Mon. Wea. Rev.,* **133,** 543–566.

Clothiaux, E. E., M. A. Miller, B. A. Albrecht, T. P. Ackerman, J. Velinde, D. M. Babb, R. M. Peters, and W. J. Syrett, 1995: An evaluation of a 94-GHz radar for remote sensing of cloud properties. *J. Atmos. Oceanic Technol.,* **12,** 201–229.

Comstock, J. M., T. P. Ackerman, and G. G. Mace, 2002: Ground-based lidar and radar remote sensing of tropical cirrus clouds at Nauru Island: Cloud statistics and radiative impacts. *J. Geophys. Res.,* **107,** 4714, doi:10.1029/2002JD002203.

DeMott, C. A., and S. A. Rutledge, 1998: The vertical structure of TOGA COARE convection. Part I: radar echo distributions. *J. Atmos. Sci.,* **55,** 2730–2747.

Dessler, A. E., 2002: The effect of deep-tropical convection on the tropical tropopause layer. *J. Geophys. Res.,* **107,** 4033, doi:10.1029/2001JD000511.

——, and S. C. Sherwood, 2000: Simulation of tropical upper tropospheric humidity. *J. Geophys. Res.,* **106,** 20 155–20 163.

——, and P. Yang, 2003: The distribution of tropical thin cirrus clouds inferred from *Terra* MODIS data. *J. Climate,* **16,** 1241–1247.

Doelling, D. R., M. M. Khaiyher, D. A. Spangenburg, M. L. Nordeen, V. Chakrapani, A. V. Gambgheer, J. Huang, and P. Minnis, 2003: The evolution of convective cloud systems determined by GOES-8 during CRYSTAL-FACE. *Proc. CRYSTAL-FACE Science Team Meeting,* Salt Lake City, UT, NASA.

Gossard, E. E., 1994: Measurement of cloud droplet size spectra by Doppler radar. *J. Atmos. Oceanic Technol.,* **11,** 712–726.

Hartmann, D. L., 1993: Radiative effects of clouds on Earth's climate. *Aerosol–Cloud–Climate Interactions,* P. V. Hobbs, Ed., International Geophysical Series 54, Academic Press, 151–173.

——, 2002: Tropical surprise (climate change causes). *Science,* **295,** 811–812.

Heymsfield, A. J., and J. Iaquinta, 2000: Cirrus crystal terminal velocities. *J. Atmos. Sci.,* **57,** 916–938.

Inoue, T., 1987: A cloud type classification with NOAA-7 split window measurements. *J. Geophys. Res.,* **92,** 3991–4000.

Jensen, E. J., O. B. Toon, W. S. Kinne, and A. J. Heymsfield, 1994: Microphysical modeling of cirrus, 1. Comparison with 1986 FIRE IFO measurements. *J. Geophys. Res.,* **99,** 10 421–10 442.

——, ——, H. B. Selkirk, J. D. Spinhirne, and M. R. Schoeberl, 1996: On the formation and persistence of subvisible cirrus clouds near the tropical tropopause. *J. Geophys. Res.,* **101,** 21 361–21 375.

Knollenberg, R. G., K. Kelly, and J. C. Wilson, 1993: Measurements of high number densities of ice crystal populations in tropical stratospheric cumulonimbus anvils. *J. Geophys. Res.,* **98,** 8639–8664.

Kummerow, C., and Coauthors, 2000: The status of the Tropical Rain Measuring Mission (TRMM) after 2 years in orbit. *J. Appl. Meteor.,* **39,** 1965–1982.

Lilly, D. K., 1988: Cirrus outflow dynamics. *J. Atmos. Sci.,* **45,** 1594–1605.

Liou, K.-N., 1986: Influence of cirrus clouds on weather and climate processes: A global perspective. *Mon. Wea. Rev.,* **114,** 1167–1200.

——, S. C. Ou, Y. Takano, F. P. J. Valero, and T. P. Ackerman, 1990: Remote sounding of the tropical cirrus cloud temperature and optical depth using 6.5 and 10.5 μm radiometers during the STEP. *J. Appl. Meteor.,* **29,** 716–726.

Liu, C. L., and A. J. Illingworth, 2000: Toward more accurate retrieval of ice water content from radar measurements of clouds. *J. Appl. Meteor.,* **39,** 1130–1146.

Luo, Z. Z., 2004: Characterizing tropical cirrus life cycle, evolution, and interaction with upper-tropospheric water vapor using Lagrangian trajectory analysis of satellite observation. *J. Climate,* **17,** 4541–4563.

Mace, G. G., and S. Benson-Troth, 2002: Cloud-layer overlap characteristics derived from long-term cloud radar data. *J. Climate,* **15,** 2505–2515.

——, A. J. Heymsfield, and M. Poellot, 2002: On retrieving the microphysical properties of cirrus clouds using the moments of the millimeter-wavelength Doppler spectrum. *J. Geophys. Res.,* **107,** 4815, doi:10.1029/2001JD001308.

Massie, S., A. Gettelman, W. Randel, and D. Baumgardner, 2002: Distribution of tropical cirrus in relation to convection. *J. Geophys. Res.,* **107,** 4591–4607.

Mather, J. H., 2003: Patterns of convection in the tropical western Pacific. *Proc. 13th ARM Science Team Meeting,* Broomfield, CO, U.S. Department of Energy.

——, T. A. Ackerman, and M. P. Jensen, 1998: Characteristics of the atmospheric state and the surface radiation budget at the tropical western pacific ARM site. *Geophys. Res. Lett.,* **25,** 4513–4516.

McFarquhar, G. M., and A. J. Heymsfield, 1996: Microphysical characteristics of three anvils sampled during the Central Equatorial Pacific Experiment. *J. Atmos. Sci.,* **53,** 2401–2423.

Mitchell, D. L., S. K. Chai, Y. L. Liu, A. J. Heymsfield, and Y. Dong, 1997: Modeling cirrus cloud. Part 1: Treatment of bimodal size spectra and cases study analysis. *J. Atmos. Sci.,* **54,** 1710–1723.

Moran, K. P., B. E. Martner, M. J. Post, R. A. Kropfli, D. C. Welsh, and K. B. Widener, 1998: An unattended cloud profiling radar for use in climate research. *Bull. Amer. Meteor. Soc.,* **79,** 443–455.

Nesbitt, S. W., E. J. Zipser, and D. J. Cecil, 2000: A census of precipitation features in the tropics using TRMM: Radar, ice scattering, and lightning observations. *J. Climate,* **13,** 4087–4106.

Petersen, W. A., and S. A. Rutledge, 2001: Regional variability in tropical convection: Observations from TRMM. *J. Climate,* **14,** 3566–3586.

Pfister, L., and Coauthors, 2001: Aircraft observation of thin cirrus clouds near the tropical tropopause. *J. Geophys. Res.,* **106,** 9765–9786.

Sherwood, S. C., 1996: Maintenance of the free-tropospheric tropical water vapor distribution. Part I: Clear regime budget. *J. Climate,* **9,** 2903–2918.

Soden, B. J., 1998: Tracking upper tropospheric water vapor radiances: a satellite perspective. *J. Geophys. Res.,* **103,** 17 069–17 081.

——, 2004: The impact of tropical convection and cirrus on upper tropospheric humidity: A lagrangian analysis of satellite measurements. *Geophys. Res. Lett.,* **31,** L20104, doi:10.1029/2004GL020980.

——, and R. Fu, 1995: A satellite analysis of deep convection, upper-tropospheric humidity, and the greenhouse effect. *J. Climate,* **8,** 2333–2351.

Spencer, R. W., H. M. Goodman, and R. E. Hood, 1989: Precipitation retrieval over land and ocean with the SSM/I: Identification and characteristics of the scattering signal. *J. Atmos. Oceanic Technol.,* **6,** 254–273.

Stephens, G. L., 2005: Cloud feedbacks in the climate system: A critical review. *J. Climate,* **18**, 237–273.

——, S. C. Tsay, P. W. Stackhouse, and P. J. Flatau, 1990: The relevance of the microphysical and radiative properties of cirrus clouds to climate and climatic feedback. *J. Atmos. Sci.,* **47,** 1742–1753.

Steranka, J., E. B. Rodgers, and R. C. Gentry, 1984: Diurnal variation of Atlantic Ocean tropical cyclone cloud distribution inferred from geostationary satellite infrared measurements. *Mon. Wea. Rev.,* **112,** 2338–2344.

Szoke, E. J., and E. J. Zipser, 1986: A radar study of convective cells in mesoscale systems in GATE. Part II: Life cycles of convective cells. *J. Atmos. Sci.,* **43,** 199–218.

Toracinta, E. R., E. J. Zipser, D. J. Cecil, and S. W. Nesbitt, 2002: Radar, passive microwave, and lightning characteristics of precipitating systems in the Tropics. *Mon. Wea. Rev.,* **130,** 802–824.

VanReken, T. M., T. A. Rissman, G. C. Roberts, V. Varutbankul, H. H. Jonsson, R. C. Flagan, and J. H. Seinfeld, 2003: Toward aerosol/cloud condensation nuclei (CCN) closure during CRYSTAL-FACE. *J. Geophys. Res.,* **108,** 4633, doi:10.1029/2003JD003582.

Williams, E., and Coauthors, 2002: Contrasting convective regimes over the Amazon: Implications for cloud electrification. *J. Geophys. Res.,* **107,** 8082, doi:10.1029/2001JD000380.

Yeh, H., and Y. Chen, 2002: The role of offshore convergence on coastal rainfall during TAMEX IOP 3. *Mon. Wea. Rev.,* **130,** 2709–2730.

Zipser, E. J., 1988: The evolution of mesoscale convective systems: Evidence from radar and satellite observations. *Tropical Rainfall Measurements,* J. Theon and N. Fugono, Eds., A. Deepak Publishing, 159–166.

——, and K. Lutz, 1994: The vertical profile of radar reflectivity of convective cells: A strong indicator of storm intensity and lightning probability? *Mon. Wea. Rev.,* **122,** 1751–1759.